JPhys Energy

TOPICAL REVIEW • OPEN ACCESS

Solution-based synthesis of kesterite thin film semiconductors

JPhys Energy

TOPICAL REVIEW

Solution-based synthesis of kesterite thin film semiconductors

T Todorov[1], H W Hillhouse[2], S Aazou[3,4], Z Sekkat[3,4], O Vigil-Galán[5], S D Deshmukh[6], R Agrawal[6], S Bourdais[7], M Valdés[8], P Arnou[9], D B Mitzi[10,11] and P J Dale[9,12]

[1] T. J. Watson Research Center, IBM Corporation, Yorktown Heights, NY 10598 United States of America
[2] Department of Chemical Engineering, University of Washington, Seattle WA 98125, United States of America
[3] Optics & Photonics Center, Moroccan Foundation for Advanced Science, Innovation & Research, MAScIR, OCP Foundation, Rabat, Morocco
[4] Department of Chemistry, Faculty of Sciences, Mohammed V University, Rabat, Morocco
[5] Higher School of Physics and Mathematics—National Polytechnic Institute, 07738, Mexico City, Mexico
[6] Davidson School of Chemical Engineering, Purdue University, West Lafayette, IN 47907, United States of America
[7] IMRA EUROPE S.A.S., 220, rue Albert Caquot, F-06904 Sophia Antipolis, France
[8] Institute of Materials Science and Technology (INTEMA), University of Mar del Plata and National Research Council (CONICET), Av. Colón 10850, 7600 Mar del Plata, Argentina
[9] Physics and Materials Science Research Unit, University of Luxembourg, Belvaux, L-4422, Luxembourg
[10] Department of Mechanical Engineering and Materials Science, Duke University, Durham, NC 27708, United States of America
[11] Department of Chemistry, Duke University, Durham, NC 27708, United States of America
[12] Author to whom any correspondence should be addressed.

E-mail: tktodoro@us.ibm.com, h2@uw.edu and phillip.dale@uni.lu

Keywords: kesterite, $Cu_2ZnSn(S, Se)_4$, solution processing, electrodeposition, nanoparticle

OPEN ACCESS

RECEIVED
2 May 2019

REVISED
7 June 2019

ACCEPTED FOR PUBLICATION
12 August 2019

PUBLISHED
9 January 2020

Abstract

Large-scale deployment of photovoltaic modules is required to power our renewable energy future. Kesterite, $Cu_2ZnSn(S, Se)_4$, is a p-type semiconductor absorber layer with a tunable bandgap consisting of earth abundant elements, and is seen as a potential 'drop-in' replacement to $Cu(In,Ga)Se_2$ in thin film solar cells. Currently, the record light-to-electrical power conversion efficiency (PCE) of kesterite-based devices is 12.6%, for which the absorber layer has been solution-processed. This efficiency must be increased if kesterite technology is to help power the future. Therefore two questions arise: what is the best way to synthesize the film? And how to improve the device efficiency? Here, we focus on the first question from a solution-based synthesis perspective. The main strategy is to mix all the elements together initially and coat them on a surface, followed by annealing in a reactive chalcogen atmosphere to react, grow grains and sinter the film. The main difference between the methods presented here is how easily the solvent, ligands, and anions are removed. Impurities impair the ability to achieve high performance (>∼10% PCE) in kesterite devices. Hydrazine routes offer the least impurities, but have environmental and safety concerns associated with hydrazine. Aprotic and protic based molecular inks are environmentally friendlier and less toxic, but they require the removal of organic and halogen species associated with the solvent and precursors, which is challenging but possible. Nanoparticle routes consisting of kesterite (or binary chalcogenides) particles require the removal of stabilizing ligands from their surfaces. Electrodeposited layers contain few impurities but are sometimes difficult to make compositionally uniform over large areas, and for metal deposited layers, they have to go through several solid-state reaction steps to form kesterite. Hence, each method has distinct advantages and disadvantages. We review the state-of-the art of each and provide perspective on the different strategies.

1. Introduction

In the context of developing a thin film photovoltaic technology that is truly scalable on the terawatt level using low-cost earth abundant elements, the kesterite semiconductor, $Cu_2ZnSn(S,Se)_4$, or CZTSSe, with a tunable bandgap between 1.0 to 1.5 eV has been a key material of interest. It may be seen as a potential replacement or

successor absorber material to Cu(In,Ga)Se_2 (CIGS), since both devices have similar architecture and processing. The key advantage of CZTSSe is the absence of indium, which may have issues with price or price volatility given its widespread use in other emerging technologies. Investigations into the use of CZTSSe for photovoltaics began in 1988 [1], and since then, it has been the subject of over 2900 publications to date. Of these publications, over 65% have investigated liquid processed layers. By this we mean that the kesterite layer was formed by annealing a precursor layer deposited from one or more solutions containing the necessary elements. Many of the advances in our knowledge of the kesterite material have come from solution-processed films, and indeed the world record power conversion efficiency (PCE) cell contains a solution processed kesterite layer [2]. Our purpose in this review is to provide a comprehensive overview of the different possible solution-based syntheses of kesterite layers by discussing the various film formation mechanisms, by giving a brief historical background for each, as well as by comparing and contrasting the latest approaches.

Solution methods to produce semiconductor precursor layers are of interest since they may be deposited uniformly at high speed, with nearly 100% material utilization, using low-capital-cost equipment. The kesterite semiconductor is synthesized by annealing a precursor layer that is formed by drying a wet film deposited from 'inks' or solutions. Although the constituents of the semiconductor, namely Cu, Zn, Sn, S, and or Se may be deposited with high purity, the challenge lies in removing all the other components of the solutions from the precursor films. Most semiconductors are notoriously sensitive to impurities, and therefore the removal of all unwanted species is a very high priority. While many CZTSSe devices achieve >8% PCE with >1 atomic% impurities (mainly carbon, nitrogen, and halogens), the best performing devices tend to have the lowest concentrations of impurities, approaching levels from vacuum-based processing. As a result, methods are sought to fabricate kesterite thin films that only contain their constituent elements with the correct composition and any necessary dopants or defect passivation agents (such as lithium and germanium).

The kesterite absorber layer can be formed from dried chemical precursor layers consisting of molecules or salts, of preformed kesterite nanoparticles, of metallic alloys, or even of binary chalcogenide compounds. This review is split into five parts covering the different possibilities. Parts (2.1) through (2.3) review the molecular and salt-based solution approaches, where different solvents may be used including: (2.1) the carbon-free solvent hydrazine, (2.2) aprotic solvents such as di-methyl-sulfoxide, and (2.3) protic solvents that may yield in-situ particle formation due to condensation reactions (the so called sol-gel method). Part (2.4) discusses the main methods to form and stabilize nanoparticles. Part (2.2) assesses the use of electrodeposition to form both metallic and metal chalcogenide precursor layers. The review is completed by (3) a brief overview of the different precursor deposition methods, and (4) associated strengths–weaknesses–opportunities–and threat (SWOT) analysis of the different solution-based synthetic routes.

2. Thin film synthesis methods

2.1. Hydrazine-Based suspensions and solutions

Ever since its conception, CZTSSe has been recognized as a challenging system for thin-film device fabrication using state-of-the-art vacuum-based methods [3]. Many exciting materials and property similarities with CIGS inspired attempts to apply analogous thin film growth approaches, such as two-step co-evaporation or sequential sputtering followed by annealing [4–6]. Composition control and secondary phase suppression during the high temperature deposition and/or crystallization is hindered in these approaches by the volatility of Sn chalcogenide phases [7], in addition to the already familiar S and Se. The process control becomes even more difficult due to the interrelation of the vapor pressure of all these three elements and their phase formation. There was therefore a need for a method that could at the same time provide precise, homogeneous target composition and facile crystallization of the desired phase, minimizing secondary phase formation and providing device-quality interfaces.

Hydrazine solution processing was the first method to simultaneously address these challenges to a level enabling CZTS to approach and later surpass the 10% PCE milestone. Despite the extreme safety precautions required for hydrazine manipulation, including flammability and toxicity, this solvent has unique properties for research on multinary chalcogenide materials. Hydrazine is carbon and oxygen-free and, due to its strong reducing properties, has the capability to form soluble chalcogenide complexes with many metals (therefore already providing desired metal–chalcogen linkages in the precursor, as needed in the final product) [8–10]. These precursors cleanly decompose at relatively low temperatures, producing highly pure crystalline layers with precise composition control. The method was first developed for SnS-based thin-film transistors [8]. Later it enabled achieving excellent composition and dopant control in some of the most sophisticated multi-element PV absorbers, such as Cu(In,Ga)(S,$Se)_2$, producing homogeneous layers with impressive crystalline quality, which were incorporated into high performance devices [9]. The efficiency was further improved to become the highest among all-inorganic solution-processed absorbers at the time (figure 1(a) [11]).

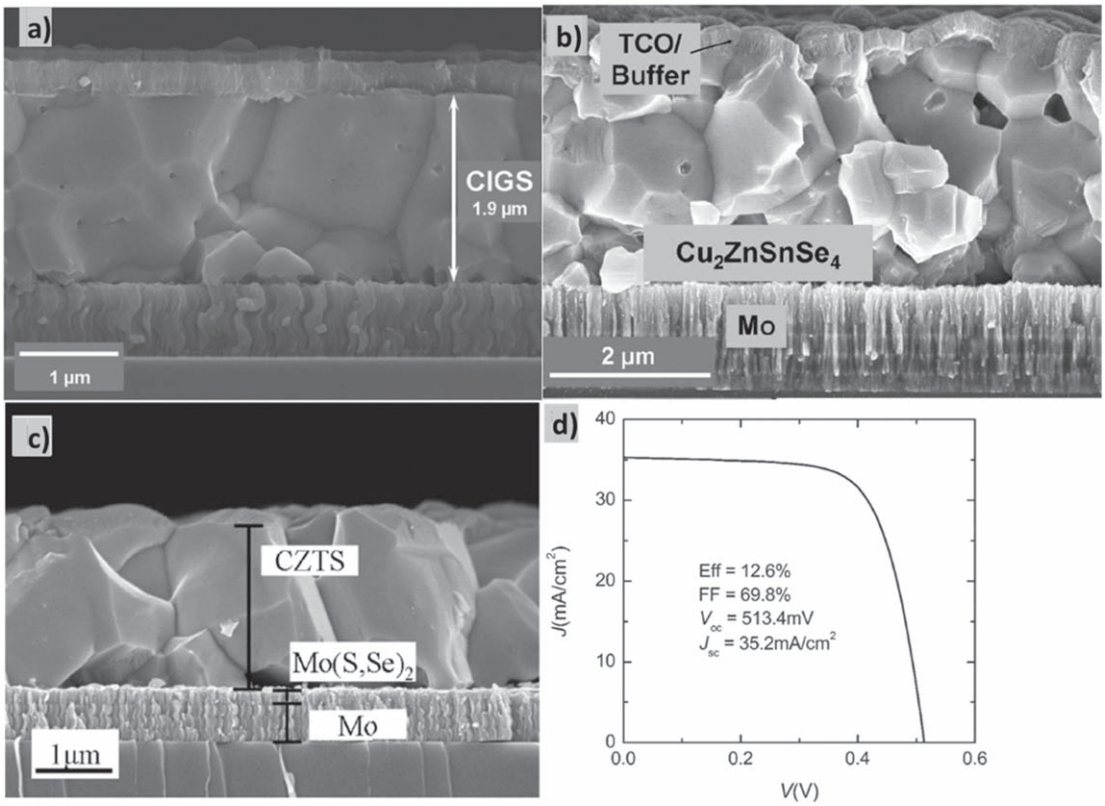

Figure 1. SEM cross sectional images of exemplary hydrazine processed absorbers: CIGS yielding 15% efficiency (a) [11], CZTS from hybrid slurry-based ink with 9.6% efficiency (b) [12], and pure-solution CZTS ink offering 12.6% efficiency (c), with corresponding *J*–*V* curve of the latter device (d) [2].

Implementation of hydrazine solution processing for CZTSSe was not straightforward, given the poor solubility of zinc chalcogenides in hydrazine (in contrast to the Cu and Sn chalcogenides). However, reaction of Zn nanoparticles with chalcogen solutions leads to the formation of zinc hydrazinate nanoparticles with different shapes [12]. These nanoparticles were found to be sufficiently dispersible in solutions of Cu and Sn chalcogenides to allow the development of hybrid solution-nanoparticle (or slurry) inks. While not yet harnessing the full reaction potential of molecularly intermixed pure solution precursors, the hybrid inks could already be spin-coated, annealed and processed, as for CIGS. Employed in analogous device structures (Glass/Mo/CZTSSe/CdS/ITO/Ni-Al, figure 1(b)), they soon yielded a breakthrough in CZTSSe performance to 9.6% efficiency [12]. This value, over 40% higher than any previous result with this material, demonstrated for the first time that an atmospheric-pressure liquid-based method was able to not only reach, but even to surpass established vacuum-based processing. The sudden boost in CZTSSe performance motivated intensified efforts to further improve this technology and dedicated projects were launched at IBM, as well as at multiple other research centers worldwide. Incremental improvements of the hybrid approach, including refinement of composition and annealing conditions to suppress Sn loss, soon increased efficiencies to >10% [13], reaching the highest PCE of 11% in 2012 [14]. Despite this success, the presence of nanoparticles and their segregation could not completely suppress localized compositional fluctuations, which limited further efficiency increase by this method.

Development of pure CZTS solutions in hydrazine relied on finding a soluble zinc precursor. This was achieved by two different routes. An approach developed at IBM used zinc formate, which could be directly dissolved in solutions containing the Cu–Sn–S–Se precursors [15]. The presence of Sn was found to be critical for the formation of soluble species, suggesting that it participated in the formation of a carboxylate complex with Zn. Independent work at UCLA used a completely different approach, which however most likely arrived at a similar soluble complex. Hydrazinocarboxylic acid, obtained by carefully reacting solid CO_2 with hydrazine, was reacted with zinc metal to form a stable complex that could be incorporated in the Sn solutions [16]. The zinc formate method soon displaced the hybrid slurry approach due to its advantages of fine composition tuning with excellent uniformity and became the main vehicle of state-of-the-art CZTS device optimization and fundamental materials understanding. Combining advanced thermal processing with precise composition and optical stack optimization of the complete device [17], a world record efficiency of 12.6% was achieved [2]. This

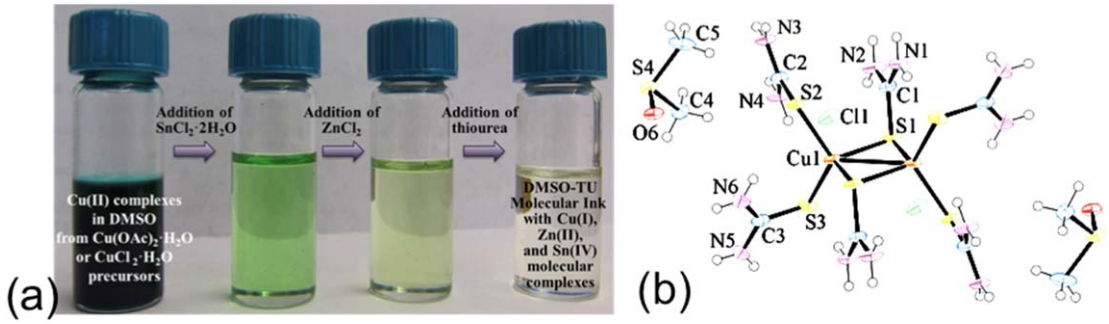

Figure 2. Molecular inks with DMSO and thiourea. (a) Sequence of steps showing the formation of a stable molecular ink for CZTS. (b) Thermal ellipsoid representation of the structure of $Cu_2(TU)_6Cl_2(DMSO)_2$ complex determined by single crystal x-ray crystallography of a crystal grown from the final ink in part (a). The structure is monoclinic space group C2/c with lattice constants $a = 23.599(4)$ Å, $b = 8.9153(15)$ Å, $c = 18.612(3)$ Å, and $\beta = 124.342(16)^\circ$, with goodness-of-fit on $F^2 = 1.119$ and wR2 = 0.096 (unpublished data (see footnote 12)).

2014 milestone remained unchallenged for many years, prompting questions as to whether CZTSSe performance has reached a plateau and if further improvement would be possible. Nevertheless, by providing state-of-the-art CZTSSe absorbers for fundamental studies, the method continued to provide key insights into the CZTSSe material and device understanding, serving as a benchmark for the improvement of a multitude of other fabrication approaches. Some of these are discussed in the following parts of this review and are already approaching and will likely surpass the long-standing efficiency milestone set by the hydrazine approach.

2.2. Aprotic molecular inks

Molecular inks are solutions—i.e. single phase homogeneous liquids, as opposed to heterogeneous mixtures, as is the case for slurries, suspensions, or colloidal dispersions of nanoparticles. A key advantage of molecular inks is that they avoid localized compositional fluctuations that are difficult to overcome with suspensions or colloidal dispersions of nanoparticles. The development of hydrazine-based molecular inks was a key advance that led to the current record CZTS device reported in 2014 (discussed above). However, hydrazine presents many challenges due to safety concerns and environmental regulations given its toxicity. As a result, molecular inks for CZTS have been developed based on other solvents, including: (1) polar aprotic solvents di-methyl-sulfoxide and di-methyl-formamide (DMSO and DMF) [18–25], (2) polar protic solvents (like water and alcohols) [26, 27], and (3) amine-thiol solutions [28–30]. Aprotic polar solvents like DMSO and DMF have very high pKa and lack a reactive oxygen site (in contrast to protic polar solvents like water and alcohols). Thus, these aprotic solvents avoid the formation of metal–oxygen–metal bonds or metal–oxygen–carbon bonds, which can be difficult to fully eliminate once formed. We also note that thiols (RSH) are more acidic (or equivalently, more protic) than their corresponding ROH alcohol. Amine-thiol routes show promise, but they must contend with a reactive hydrogen that may yield difficult to remove MSR functional groups that result from condensation reactions with the thiol (RSH). In this section, we focus primarily on the aprotic polar solvent route to molecular inks.

A widely studied molecular ink route to CZTS is based on the relatively benign aprotic polar solvent DMSO and a sulfur containing complexation ligand thiourea (TU), which was first reported in 2011 [18]. In DMSO, the hydrogens on TU are not very acidic (note that the pKa of TU in DMSO is 21) [31]. As a result, TU tends to act as a ligand to solvate metal cations with the accessible soft Lewis base S-donor site coordinated to the metal cation. In fact, many TU-metal complexes for soft metal cations are well-known and studied, including $CuCl(TU)_3$ [32], $Cu_2Cl_2(TU)_4$ [33], $AgCl(TU)_2$ [34], $ZnCl_2(TU)_2$ [35], and $SnCl_2(TU)$ [35]. For the CZTS system, single crystals of $Cu_2(TU)_6Cl_2(DMSO)_2$ (figure 1(b)) have been isolated from complete inks (figure 2(a), far right)[13]. Further, with DMSO as the primary solvent, hydrated metal salt complexes can be used as precursors since even water in DMSO is quite aprotic with a pKa of 31.4 [36]. In fact, experiments show that DMSO can often be replaced with H_2O at up to 50 vol% in the parent solvent without triggering hydrolysis and condensation reactions that lead to conventional sol-gel chemistry (see footnote 12). The use of water may be desirable to make the solvent and ink even more 'green'.

The desired oxidation state for cations in CZTS (+1, +2, and +4 for Cu, Zn, and Sn, respectively) may be achieved in the molecular ink by dissolving salts where the metals are already in that oxidation state [21, 22, 24] or by adding salts with metals in other oxidation states, provided that they have a facile pathway for redox reactions to reach to the desired oxidation state. This latter approach is exemplified by Xin *et al* [19], in which

[13] Hillhouse group result previously unpublished.

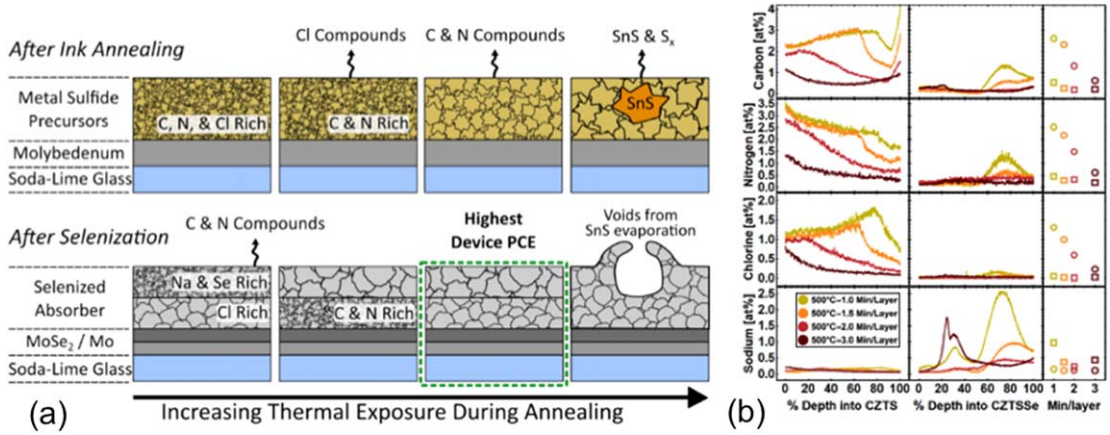

Figure 3. (a) Schematic showing the effects of thermal exposure during annealing and selenization and their effect on bilayer formation, impurity removal, and the formation of dense grains (adapted from Clark *et al*) [47]. (b) Composition-calibrated glow-discharge optical emission spectroscopy (cc-GDOES) depth profiles showing the sensitivity of impurity removal to the annealing profile. Specifically, it shows that 3 min anneal at 500 °C after the deposition of each layer is sufficient to remove carbon, nitrogen, and chlorine down to close to the detection limit after selenization.

Cu(II) and Sn(II) precursors are added to the DMSO solution (without TU present) and undergo a redox reaction, $2Cu^{+2} + Sn^{+2} \rightarrow 2Cu^{+1} + Sn^{+4}$, as indicated by the transition from a dark-green tinted solution due to Cu(II) to a colorless solution indicative of Cu(I) (figure 2(a)). The additional chloride that accompanies the $SnCl_2$ and $ZnCl_2$ also has a beneficial effect, in allowing the formation of a DMSO-soluble copper chloride anion $(Cu_4Cl_6)^{-2}$, as determined by single crystal x-ray structure solution of crystals to be $Zn(DMSO)_6^{+2}(Cu_4Cl_6)^{-2}$. The crystals were grown by evaporating DMSO from the ink after $ZnCl_2$ addition. Upon addition of TU to the ink, Cu(I) forms a complex with the TU yielding a stable molecular ink. Single crystal x-ray structure solution of the first crystals that formed upon DMSO evaporation from the complete ink, are determined to be $Cu_2(TU)_6Cl_2(DMSO)_2$, as shown in figure 1(b). In contrast to the soft Cu(I) cation, the harder Zn(II) and Sn(IV) preferentially complex with the harder O-donor Lewis base site on DMSO and the O-donor and N-donor Lewis base sites on DMF. Later, Clark *et al* [37] showed that chloride transfer reactions are extremely common and useful for forming kesterite and chalcogen semiconductor films. Further, by expanding the aprotic solvent suite to include DMF, Clark showed that an even wider variety of metal cations (useful for kesterites more broadly) can be stabilized. Some metal species including Ag(I), Ge(II), and Ge(IV) (which are studied in an attempt to reduce cation site disorder in the kesterite lattice) [38–43] have low solubility or low stability in DMSO-TU inks, and can be stabilized by molecular inks based on DMF and TU. Overall, this research illustrates that DMSO-TU and DMF-TU solutions are very flexible chemical routes to solvate a wide spectrum of metal chloride salts due to a variety of soft and hard Lewis base sites available to accommodate both soft cations like Cu(I), Ag(I), and Sn(II) and harder cations like Cu(II), Zn(II), Sn(IV), and Ge(IV).

One of the key challenges to making high quality kesterite semiconductors from any molecular ink is the removal of impurities. For the DMF-TU and DMSO-TU inks, these impurities are primarily carbon, nitrogen and chloride compounds. While there are several pathways that lead to dense large-grain crystalline films, there are many reports of CZTS films from these molecular ink processes that exhibit multilayer morphologies [44–46]. These morphologies often show a fine-grained impurity-rich layer trapped in between dense, larger-crystalline grains and the substrate. Using composition-calibrated glow-discharge optical emission spectroscopy (cc-GDOES) to reveal the depth-dependent concentration of impurities (see figure 3), it was shown that the process parameters of the annealing and selenization steps are critical to avoid the trapping of impurities. Intermediate annealing temperatures led to the formation of amorphous hydrogenated carbon nitride (a-C:H:N) from the polymerization of TU decomposition products [47]. These impurity-rich layers could be avoided in two ways: (1) by using low annealing temperatures that prevent extended a-C:H:N networks from forming and allow the C and N compounds to be volatilized during subsequent selenization, and (2) by using high annealing temperatures where the a-C:H:N thermally decomposes during annealing (before selenization) [47]. Other parameters, such as film thickness and the alkali environment during selenization also have a major impact on the extent of impurity removal.

The DMSO-TU and DMF-TU chemistry has led to some of the highest quality films and highest PCEs devices for CZTSSe, fabricated by spin coating followed by annealing and selenization (figure 4(a)). In 2015, the DMSO-TU chemistry was used to incorporate lithium doping into CZTS inks, which led to dense impurity-free absorbers (figure 4(b)) and yielded 11.8% active area PCE devices [20]. The DMSO-TU route was also studied by

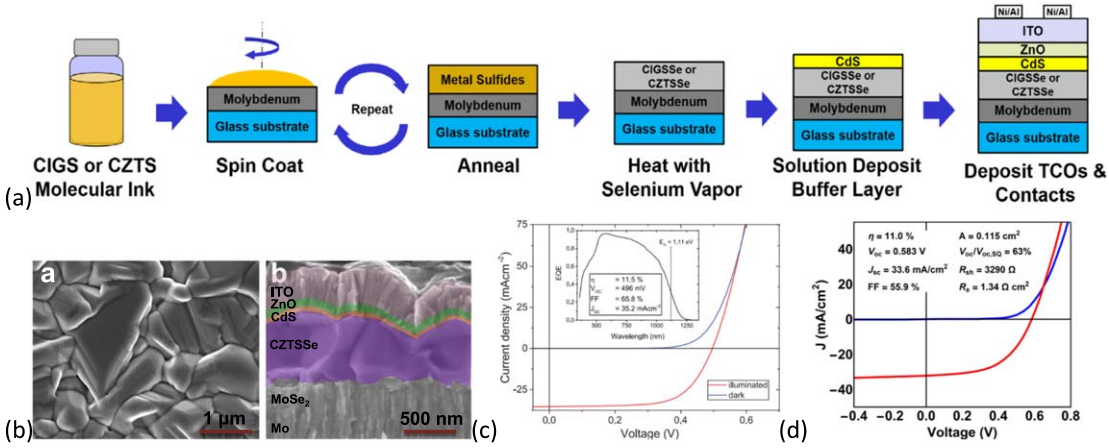

Figure 4. (a) Schematic of device fabrication with molecular inks. (b) Top surface of CZTSSe film from DMSO-TU molecular ink after selenization and cross-section of a ~11% PCE device (adapted from Xin *et al*) [20] (c) highest performance cell from DMSO-TU molecular ink at 11.5% total area PCE with 12.3% active area PCE, adapted from Haas *et al* [49] (d) *J–V* of a germanium alloyed CZTGSSe device from the DMF-TU molecular ink process which shows the highest reported $V_{oc}/V_{oc,}^{SQ}$ for any kesterite device [22] of 63%.

groups at ZSW [44] and Empa [48], each reporting devices with >10% PCEs. More recently in 2018, Haas *et al* [49] presented a large study of over 700 CZTS devices from DMSO-TU inks, examining the effects of Li, Na, Cs, and Rb doping and the cross-correlation with the metal ratios. The same study also found that Li yielded the best devices and reported a new record of 12.3% active area PCE for hydrazine-free CZTSSe figure 4(c) [49]. Also, the DMF-TU system has been used to spray-coat germanium-alloyed CZGTSSe devices [22] with 11.0% PCE and a record high open circuit voltage (V_{oc}) of 583 mV for the 1.15 eV bandgap, which is 63% of the Shockley–Queisser (SQ) limit V_{oc}. This is the highest $V_{oc}/\ V_{oc}^{SQ}$ reported for any kesterite-based device with any bandgap, including the record hydrazine-based devices [2] that only reach 58% of their SQ V_{oc} limit. These percentages are calculated by dividing the measured V_{oc} by the calculated SQ V_{oc} for the bandgap, which is a much more transparent way to quantify the voltage performance for a variable bandgap material, like CZTS. This is in contrast to simply using the measured V_{oc} or even the concept of a voltage deficit, since both values depend on bandgap. Using either V_{oc} or V_{oc} deficit can often be misleading about the voltage performance [22]. Our previously reported detailed balance calculations show that the SQ V_{oc} in units of volts is linearly related to bandgap in units of electron-volts with $V_{oc}^{SQ} = 0.932 \times \mathrm{Eg} - 0.167$, which can then be used to calculate the percentage, $100 \times V_{oc}/V_{oc}^{SQ}$ [22].

2.3. Protic solvents and the sol-gel method

The sol-gel method is a solution-based synthesis technique where one first forms a colloidal suspension of solid particles (a 'sol'), which then undergoes gelation (gel). The resulting gel is a continuous network of connected solid phase particles in a secondary continuous phase, usually a liquid. The predominate reaction mechanisms are hydrolysis of the metals followed by poly-condensation reactions [50, 51]. The 'sol-gel' method provides a facile and promising route towards low-cost mass production, which allows for precise control over the microstructure and the film composition.

The sol-gel technique involves three steps for the preparation of thin films. In the first step, the metals are dissolved as ions into solution using precursors such as copper (II) acetate monohydrate, zinc (II) acetate dihydrate and tin (II) chloride dihydrate [50, 52]. The solvent is typically 2-methoxyethanol [52] and a stabilizer such as monoethanolamine can be added [50]. Additionally, a sulfur source in the form of thiourea, may be added to the solution [52]. As also described in the aprotic solvent part (2.2) above, thiourea may complex with the metal ions in solution. The chosen salts must completely dissolve and be stable for hours. Any precipitation will lead to a change of bulk solution composition, changing the final kesterite layer composition. If the precipitates get into the final layer, they will form secondary phases within the absorber layer. The second step consists of kesterite precursor thin film formation, which involves (i) spin coating the solution near to room temperature onto a molybdenum-coated glass substrate (ii) a baking process in air using a hot plate to form the metal oxides and remove the residual impurities, and (iii) repeating the coating/baking cycle several times to reach the appropriate thickness of the absorber. The coating solution must not react with the molybdenum, and the film has to be smooth and pinhole-free, since otherwise the solar cell efficiency will be likely deteriorated by shunting. In the final third step, a high temperature thermal treatment in a reducing and/or an aggressively chalcogenizing environment is required to produce the desired CZTSSe phase, remove oxygen and other

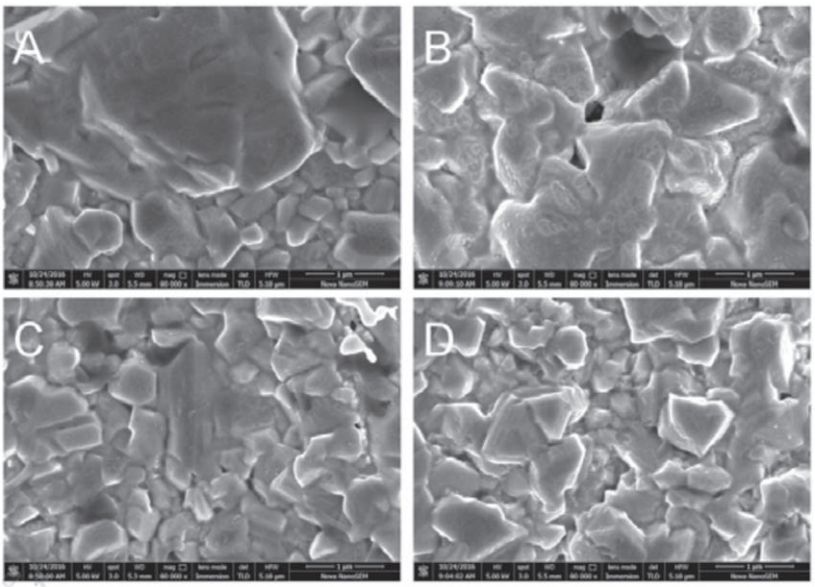

Figure 5. Top view SEM images of the samples A, B, C and D as described in the text below[53].

impurities, and create crystalline material. During this stage, gas-solid reactions take place at the surface, as well as solid-state reactions in the bulk between the elements, which lead to binary, ternary and finally quaternary chalcogenides. The annealing temperature and atmosphere play a key role in determining the composition and crystallite grain size.

Recently, Sun *et al* demonstrated a CZTS based solar cell with 8.8% PCE using the solvent, stabilizer and precursors described above [53]. They investigated the solar cell efficiency dependence on the initial metal solution concentrations by varying the Cu/Sn ratio in the following way: 1.69, 1.78, 1.84 and 1.93 labeling the samples A, B, C and D, respectively, while keeping the Zn/Sn = 1.25, S/Metal = 2 in the precursor constant [53]. The resulting kesterite absorber layer films are illustrated in figure 5. The best cell was achieved with film C, yielding a high V_{oc} of 746 mV, whilst the solar cells A and B were shunted [53]. In a previous work [54], Cu_2ZnSnS_4 kesterite-based thin films were successfully prepared using copper acetate (1.6 M), zinc acetate (1 M), tin chloride (0.8 M), and thiourea (6.4 M) using 2-methoxyethanol as a solvent, where the authors studied the effect of the film thickness on the kesterite structural and optical properties. Based on the XRD and Raman characterization, it was found that the crystalline quality was improved with increasing film thickness. A bandgap of 1.43 eV was observed for the thickest film with the highest crystallinity. They also noticed that, by increasing the total annealing pressure, a secondary phase SnS_2 can be formed.

2.4. Nanoparticle-Inks

Reviews can be found on fabricating nanoparticles (NPs) of various types (e.g. metallic, chalcogenides, oxides) for application in different locations of thin-film photovoltaic devices [55], on the approach of using sintered NPs for CIGS or CZTS [56], and on the evolution of NP-based CZTS device efficiency [57]. Here, we provide an update and comprehensive survey on the CZTS nanoparticle processing.

Nanoparticle-based inks provide the option to distinguish between the solvent(s) used for precursor dissolution and NP synthesis, from the solvent(s) used for NP deposition. This may allow for better processing control (e.g. lower residual contaminants or viscosity adjustment), such as NPs rinsing, protection with shorter ligands, mixing NPs with varying composition and/or size distributions, prior re-formulation in a new, e.g. less toxic solvent. As illustrated in figure 6, precursor film formation from nanoparticles generally proceeds in three steps: (A) colloidal synthesis of solid nanoparticles, (B) re-formulation into an ink, (C) coating into a porous film. Even though a high temperature crystallization step under chalcogen atmosphere ($T > 400$ °C, under S and/or Se) is generally required after deposition, the final metal chalcogenide composition can be fixed from the start. CZTSSe device efficiencies in the 9%–11% efficiency range have been demonstrated with the desired Cu-poor, Zn-rich metallic ratios, thanks to fine compositional tuning from the initial precursor solutions [58–60]. Below, the three steps are discussed in more detail.

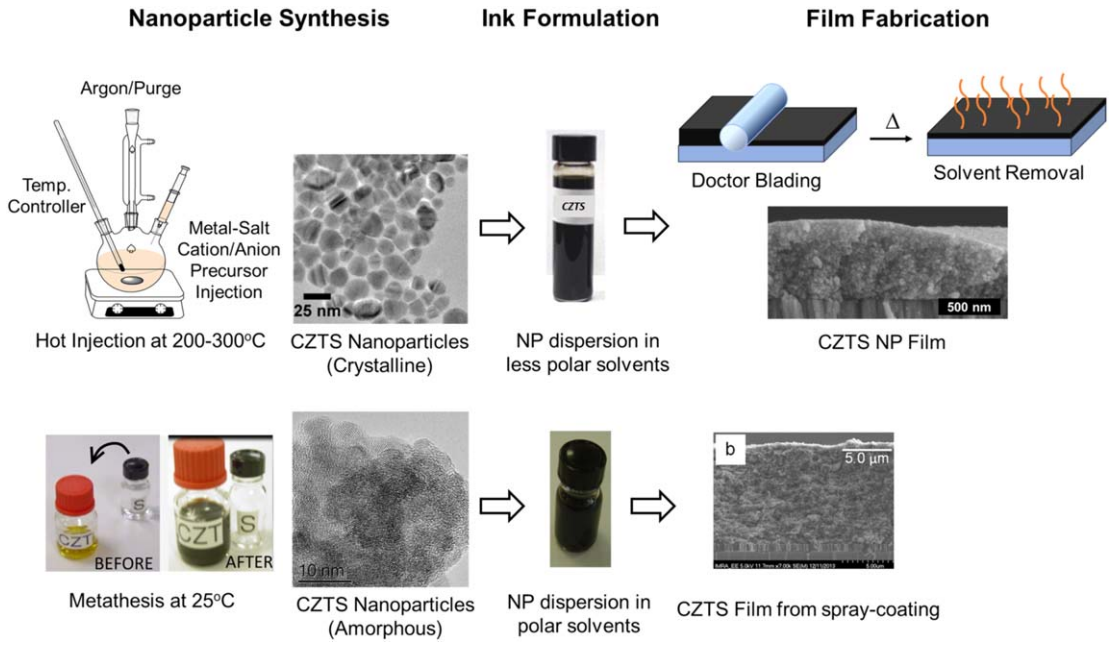

Figure 6. *TOP*: Hot injection synthesis method. TEM views of Cu_2ZnSnS_4 nanocrystals (After Ford *et al*, 2011) [40] and SEM cross-section view of NP film deposited by doctor blading technique on Mo substrate (After Hages and Agrawal, 2015) [61] *BOTTOM*: Metathesis reaction at room temperature. TEM view of the resulting amorphous CZTS nanoparticles (After Bourdais *et al*, 2012) [62] and cross-section view of NP film deposited by spray-coating on Mo substrate (After Larramona *et al* 2014) [63].

2.4.1. Particle synthesis

At least two different reactant solutions are needed for NP formation. Depending on their mixing conditions (nature of solvents, precursor concentrations, additives, time, and of prime importance the temperature), the reaction can result either in well-crystallized or amorphous-like NPs.

The first CZTS nanoparticles were reported in 2009 by various groups based on a high temperature non-aqueous co-precipitation method [64–66], similar to CIGS NPs reported in 2008 [67]. This non-aqueous hot injection (HI) method is the most abundant in literature. Previous reviews and perspectives on kesterite NPs and associated CZTSSe devices can be found in Bucherl *et al* [56] from 2013, Ghorpade *et al* [68] from 2014, and Hages and Agrawal [61] from 2015. In a typical reaction, for the synthesis of CZTS nanocrystals as reported by Guo *et al* [64], oleylamine (OLA) serves as surfactant and solvent to dissolve cation precursors at temperatures of around 225 °C. The nanoparticle nucleation is initiated by injecting a 'S dissolved in OLA' solution into a pre-heated cation solution, and these nuclei are allowed to grow by maintaining the elevated reaction temperature for a certain period until the desired particle size is achieved (typically 0.5–1 h). These OLA-capped nanoparticles after proper washing are then dispersed in the desired solvent to formulate a nanocrystal ink for coating films. Riha *et al* have reported a slight variation to this route, which involves use of tri-octyl-phosphine oxide (TOPO) as a solvent along with OLA, giving better particle monodispersity. Another similar synthesis of CZTS nanoparticles is achieved via the heat-up route, for which cations and S are mixed together in OLA and heated to a reaction temperature of around 280 °C, to yield monodisperse CZTS nanoparticles and to avoid the need for HI. Along with pure CZTS nanoparticle synthesis, the HI process has also been successful in synthesizing cation-alloyed CZTS nanoparticles, including Ge-doped CZTS [69, 70] and Ag-doped CZTS [71], by using corresponding metal precursors for the reaction, and has shown improved photovoltaic performance compared to pure CZTS nanoparticle devices [59, 71]. The CZTSe layers in high efficiency devices generally exhibit the kesterite crystal structure, but NP synthesis of CZTS materials can also yield a meta-stable wurtzite phase, e.g. through the choice of solvent, such as dodecanethiol [72, 73], which can then be converted into the kesterite phase by performing an annealing step under Se environment [74].

The Metathesis method (also called instantaneous precipitation) is another route to synthesize nanoparticles and is performed at room temperature or even within an ice bath. Applied initially for instance to MoS_2 [75], CdTe and Cu(In,Ga)Se_2 [76], this approach often results in NPs with comparatively poor crystallinity. A similar room temperature process for Cu_2ZnSnS_4 NP metathesis was later reported by IMRA Europe in 2014 [62, 63], based on comparatively benign solvents (water and acetonitrile). This approach is also applicable to a range of sulfide compounds, such as Sb_2S_3 or SnS [62]. In a typical CZTS metathesis, a de-oxygenated aqueous solution of NaHS is poured into an acetonitrile (CH_3CN) solution of the three metal chlorides $SnCl_4$, $ZnCl_2$ and CuCl. Performed under ambient conditions (preferentially under nitrogen), the mixing instantaneously results in an

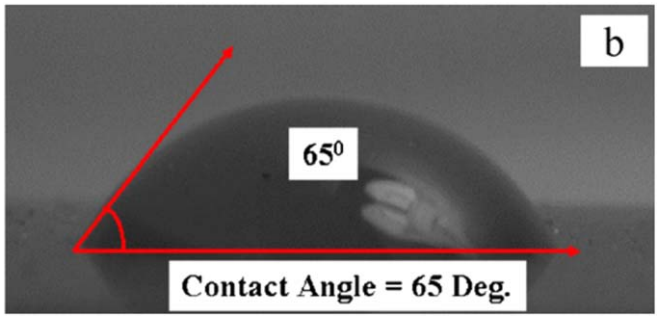

Figure 7. Contact angle measurement of water drop on annealed CZTS thin film (after Shinde *et al* 2011) [80].

aqueous colloid comprised of amorphous-like nanoparticles, with a size $<$ 10 nm (figure 6, bottom). In these round nanoparticles, TEM EDS indicated that the four elements Cu, Zn, Sn, S are intimately mixed at tunable compositions, together with traces of Na; the latter being (intentionally not completely) removed afterwards by water rinsing steps prior formulation.

Although, use of the nanoparticle HI approach suggests nanoscale film uniformity, a STEM-EDS study by Yang *et al* shows inter-particle (within a single particle) and intra-particle (between two particles) compositional non-uniformities for CZTS nanoparticles synthesized from various recipes involving the HI approach [77]. This compositional non-uniformity, which also extends to non-uniform CZTS nanoparticle size distribution, can be reduced to some extent by increasing the reaction temperature and time [70, 78]. Films casted using such non-uniform particles exhibit composition variation across the film but reactive annealing performed in a selenium environment at temperatures above 400 °C results in redistribution of the elements and ultimately relatively uniform CZTSSe film composition [77].

2.4.2. Formulation

As illustrated above, nanoparticles for fabricating CZTSSe active layers are generally synthesized as pure sulfide NPs. Indeed, to our knowledge, >9% PCE devices have been demonstrated only with films based on pure-sulfide NPs and with the S/Se ratio adjustment being performed during the high temperature selenization of the porous films from deposited/dried ink. Nanoparticles synthesized using the HI approach generally yield OLA capping on the particle surfaces, which requires the use of non-polar or low polarity solvents like hexane, toluene and hexanethiol, in order to disperse the particles for ink formulation [79]. However, an advantageous characteristic of the sulfur-terminated CZTS surface is its good wettability with water (figure 7) [80]. At the ink formulation stage, pure-sulfide NPs that were fabricated from metathesis can thus be dispersed as stable inks into water, and more generally into polar solvents (figure 8). This flexibility offers a broad range of solvents for ink formulation, including environment-friendly solvents [62].

2.4.3. Deposition methods

Porous film deposition from NP-based inks simply involves the controlled evaporation of the solvent during deposition (either by spin coating, doctor blading, spraying or cousin coating methods - see the overview of coating methods in section 3), nominally without the concern of removing by-products seen in reactive deposition methods, like spray pyrolysis [81]. For photovoltaic thin film absorber application, a final thickness of 1–2 μm is needed, which in any case implies the need for repeated coating steps (from two to ten steps). Typical film fabrication for OLA-capped CZTS NPs using the doctor blading technique involves dispersion of NPs in hexanethiol solvent with mass concentration between 200 and 300 mg ml^{-1}, which results in ~1 μm thick films with two consecutive coatings. Each coating is generally followed by an annealing step at around 300 °C to remove the excess solvent from the layer, yielding a porous nanoparticle film [78].

Non-reactive spray deposition of porous films from inks made of inorganic nanoparticles (metathesis) has been reported for e.g. CIGS [76], CdTe [82] or CZTS [63]. In the latter case, the formulation ink (10 mg ml^{-1}) was diluted in a mixed 90% water/10% ethanol solvent, a ratio that was adjusted for optimum evaporation rate during spray deposition (at a temperature of ~300 °C). To make the approach successful for photovoltaic applications, the subsequent conversion of such porous films (figure 9) into a dense CZTS film with large grains (on the order of the film thickness) is critical. In contrast with the case of sprayed Cu(In,Ga)Se_2 films, which always resulted in poor morphology and <5% PCE when starting from NPs [83], large CZTS grains could be achieved by annealing under nitrogen, with PCEs of 5%–7% for the corresponding devices. The likely reasons for this achievement are the absence of carbon-containing ligands, an oxidation-reduction reaction between Sn from CZTS NPs and the Mo substrate [63] and the presence of Na traces. A second annealing step under Se

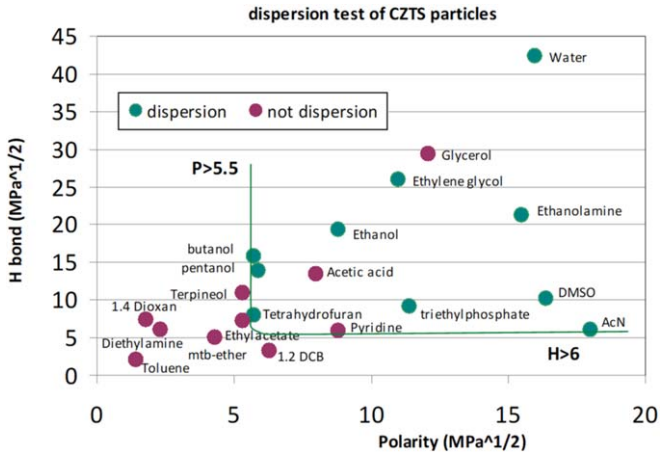

Figure 8. Solvent selection criteria for stable CZTS colloids made of CZTS NPs (metathesis method) re-dispersed in various solvents, at 5 mg ml^{-1} concentration. Green dots correspond to colloidal dispersions that have not sedimented after 24 h, at ambient temperature. Each tested solvent is characterized here by two Hansen Solubility Parameters: its hydrogen bond δ_H and polarity δ_P parameters (unpublished data)[14].

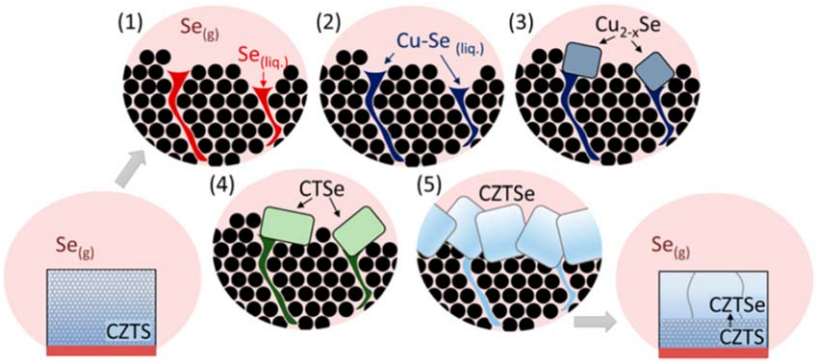

Figure 9. Diagram of the proposed liquid-assisted growth mechanism for large-grain CZTSe absorbers from CZTS nanoparticle films [85].

atmosphere was then developed, among other refinements, to form CZTSSe films (~65 at% Se-rich) with 9%–11% record PCEs [58, 84].

Typically, a selenization is used to convert the CZTS (amorphous or crystalline NPs) film into a CZTSSe layer containing large grains. This process occurs via liquid-assisted growth, in which the film is identified to undergo a sintering mechanism that involves (figure 9): (1) condensation of Se in the CZTS NP film (2) dissolution of Cu in liquid Se (3) nucleation of $Cu_{2-x}Se$ grains on the surface (4/5) incorporation of Sn/Zn via transport through liquid phase/solid-state diffusion as shown in figure 9 [85].

2.5. Electrochemical coating

Among non-vacuum technologies for metal film formation, electrodeposition stands out as a mature technology and one of the most effective, as well as low-cost, in industrial sectors worldwide. For the semiconductor sector, it has been used successfully by BP for the commercial deposition of CdTe thin film PV modules and in other PV technologies [86]. Since the pioneering work published by Scragg *et al* [87], more than 150 papers have been dedicated to the electrochemical preparation of kesterites, including several review papers [88, 89].

As a shared feature with other coating methods, the classical 2-stage approach employed for the synthesis of kesterite films remains for electrochemical routes, which involves an electrodeposited precursor film followed by chalcogenization. It is in the precursor deposition stage where different electrodeposition routes have been targeted. There are different ways of classifying the electrochemical approaches used to date. One way is to

[14] Chone C, Bourdais S and Dennler G, IMRA Europe previously unpublished.

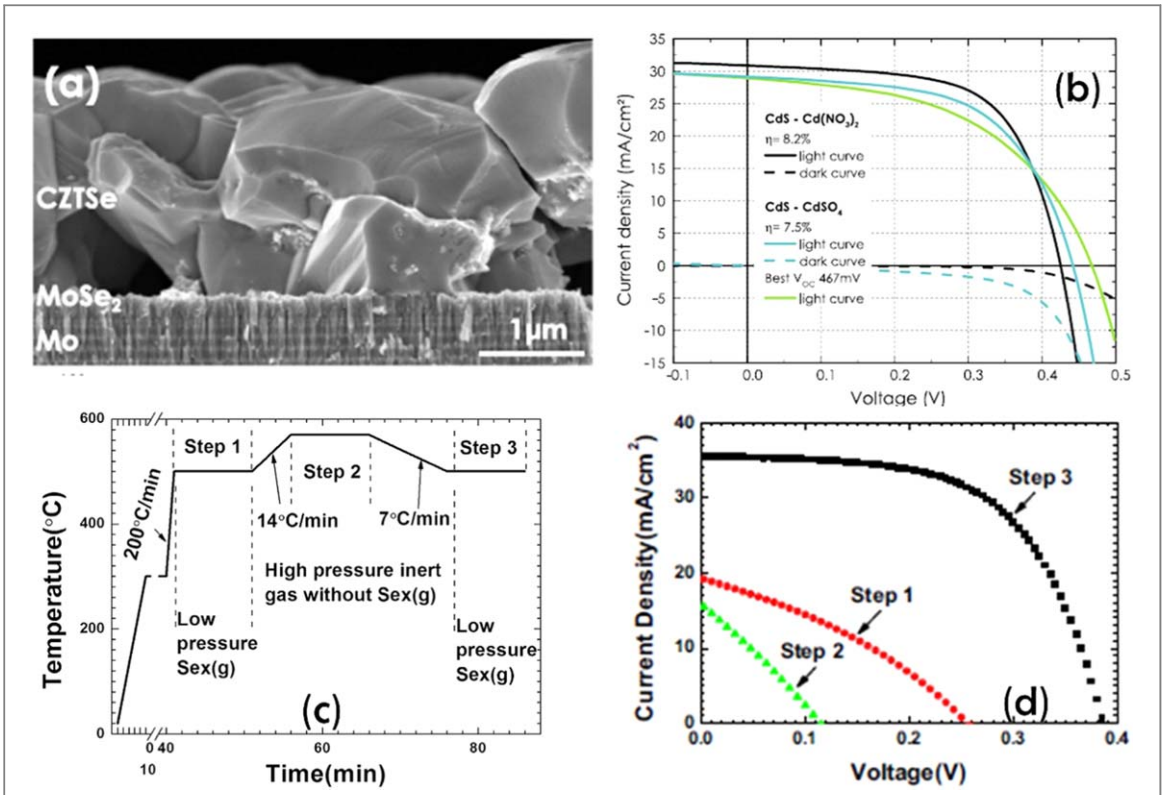

Figure 10. Top efficiencies of kesterite PV cells reported by the SEL approach. (a) SEM cross-section of selenized Cu/Sn/Zn stack (b) 8.2% CZTSe device after buffer layer optimization (after Vauche *et al* [96]). (c) Temperature profiles of three-step selenization process and (d) 8.2% CZTSe solar cell with optimized three-step selenization process (after Yao *et al* [97]).

differentiate them according to the number of 'electrochemical' steps (or number of electrodepositions) required for the deposition of the precursor. According to this classification scheme, two approaches can be differentiated. The first approach contains those methods where multiple layers are electrodeposited to form the precursor. This group comprises the stacked elemental layer (SEL) method and includes the sequential electrodeposition of elemental metallic layers [87, 90, 91], sequential electrodeposition of stacked alloys in the form of CuZn/CuSn [92], and a combination of these, involving the successive electrodeposition of elemental and binary metallic layers [93, 94]. The second approach involves those methods where one single electrochemical step is used to form the precursor. This group includes the co-electrodeposition method involving the deposition of a CuSnZn compound; and the so-called 'one pot' electrodeposition where the chalcogen source (selenium or sulfur) is also incorporated in the electrolyte, with the aim of directly obtaining CZTS or CZTSe. A comprehensive review of most of these electrochemical approaches was previously published by Colombara and coworkers [89]. In light of this, this section will focus on more recently published work so as not to duplicate past review efforts. Recent progress in terms of material quality, new insights and solar cell performance will be highlighted for each methodology.

2.5.1. Multiple layer deposition

The sequential electrodeposition of metallic layers has historically been the approach that leads to the highest PCEs [91, 95]. An 8.2% record PCE for pure selenide kesterites has been achieved so far. First, Vauche *et al* [96] have reported this result for large area electrodeposited Cu–Sn–Zn stacked precursors, followed by selenization. A remarkable improvement in device performance was attainable after the incorporation of etching procedures (for removal of zinc and tin selenide secondary phases) and buffer layer optimization (figures 10(a) and (b)). Soon after, Yao *et al* [97] achieved the same efficiency by optimization of the selenization process and without etching steps. A three-stage annealing at low Se-pressure prevents tin loss and the formation of a thick $MoSe_2$ layer, thereby enhancing the device efficiency. In terms of sulfurized SEL precursors (CZTS), a record PCE of 8.1% was reported by Jiang *et al* [98, 99]. The authors point out the significance of a long preheating treatment (≈200 min) of the electrodeposited Cu/Sn/Zn stacks, in order to achieve the highest quality of CZTS films and PV devices (figures 1(c) and (d)).

More recent contributions for the SEL approach have been focused on replacing water electrolytes by non-aqueous solvents. For instance, ionic liquids usually offer higher temperature operation and expand the electrochemical potential window making possible the use of higher current densities during electrodeposition

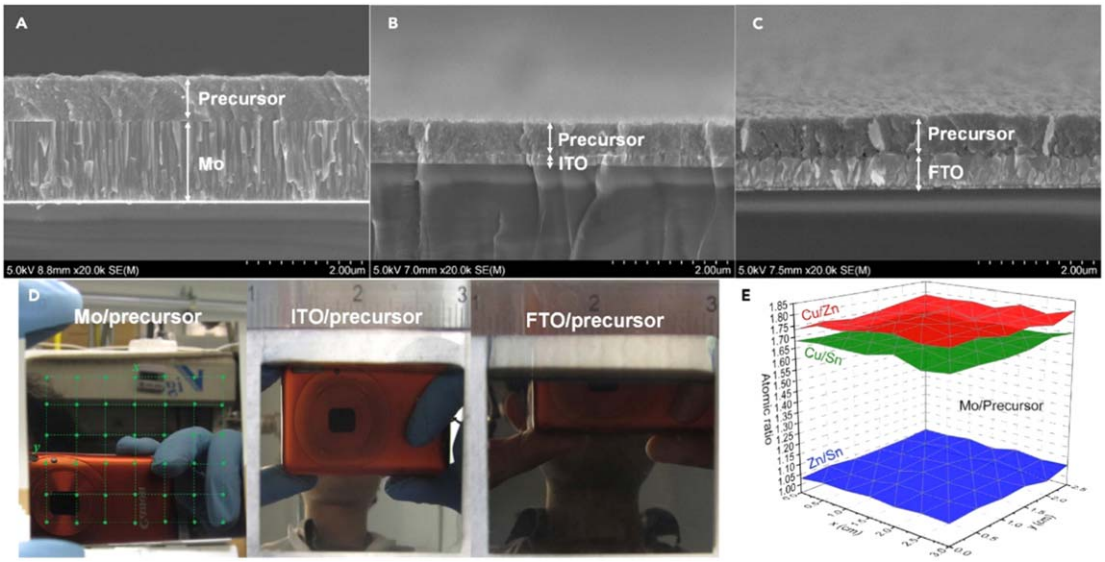

Figure 11. Uniformity evaluation of one-step CZTS electrodeposited precursors on Mo, ITO, and FTO substrates (2 × 2 inch size). (A)–(C) cross-section SEM images on different substrates (D) photographic pictures of mirror-like CZTS precursors showing the grid used to record 42 EDS measurements in the precursors (6 × 7), and (E) element distribution of the precursor on Mo substrate (after Ge *et al* [116]).

because no competing electrochemical hydrogen evolution (reduction of protons) occurs [100]. Recently, Steichen and coworkers have reported a high speed electrochemical SEL procedure achieving average metallic deposition rate of 100 nm s^{-1} through the use of liquid metal salts [101]. This SEL approach combined with a rapid thermal process (RTP) is capable of producing a promising 5.5% CZTSe PV device.

The synthesis of Ge-alloyed kesterite films has also been explored for higher bandgap using multilayer electrodeposition [102]. In this work brass/tin/germanium stacks were prepared, using pyrophosphate electrolytes for brass and tin electrodeposition and an organic electrolyte for Ge electrodeposition. Despite only minor improvement in terms of PCE, this first attempt expands the capacity of electrochemical methods to obtain kesterites of varied compositions.

2.5.2. Compound electrodeposition

In the last years, most of the published works related to co-electrodeposition have addressed the replacement of citrate salts [103–105] as a complexing agent by pyrophosphates [106–108]. Other work has studied the effect of cell configuration on the compositional homogeneity of electrodeposited Cu–Zn–Sn alloys [109]. Also, sulfurized and selenized compound electrodeposited precursors were successfully tested in other types of PV devices, like DSSCs [110] or photocathodes for water splitting [111]. In terms of PCE, the record for the co-electrodeposition approach is still 8.0%, as reported by Jeon and coworkers [112]. More recent contributions have explored the combination of this approach with a RTP annealing, which is more attractive from an industrial perspective, and reported a 5.2% PCE [113].

The use of a quaternary-salt containing electrolyte has been the approach that has progressed the most in terms of increasing device efficiency. From a 5.5% PCE reported by Ge *et al* [114] in 2014, a new record 8.7% PCE CZTS solar cell has been recently reported by Zhang and coworkers [115]. Similarly, Ge *et al* have improved their previous solar cells by reporting a 7.1% CZTS PCE. In this work, after a systematic investigation, refined plating parameters and an optimized electrolyte led to the obtaining of electrodeposits with outstanding layer uniformity in terms of film appearances and compositions, of comparable quality to those obtained by vacuum-based methods (figure 11).

3. Overview of coating methods

CZTSSe absorbers have been deposited from liquid-based precursors using a large range of deposition techniques. The quality of the final material is affected by all process parameters, such as compositional control, extrinsic doping or annealing parameters, in a rather complex way. Nonetheless, the deposition method itself is highly important, since compact and uniform layers (both in terms of thickness and stoichiometry) are required to obtain high performance solar cells in the subsequent steps. For a uniform and crack-free coating, the deposition method should be carefully combined with an ink that exhibits the appropriate rheological

properties, such as the viscosity, density and surface tension. The compactness of the film must be maintained after any intermediate drying step, which is performed to evaporate the solvent and remove impurities. Drying of the film often results in the formation of cracks, which can act as shunting paths in the solar cell and reduce its performance. To eliminate this effect, the absorber is typically deposited through a series of deposition/drying cycles, such that the deposited film does not exceed a 'critical' thickness, related to the tensile strength and the Young's modulus of the film [117].

Typical deposition methods for CZTSSe thin films involve two separate steps—i.e., the material coating followed by a post-deposition step, in the form of a thermal or chemical treatment. The processes where the high quality material is obtained in a separate step from the coating, have also been referred to as sequential or 'two step' approaches [118]. The benefit of sequential approaches is that the deposition step can be performed using a low capital cost method and/or at rather low temperatures. The ideal deposition method would have a low thermal budget, high deposition rates and low operating costs to be industrially relevant. This section will give an overview of the most popular coating methods for research-scale CZTSSe precursor layer deposition, and the highest PCE values for the given methods are compared in table 1.

3.1. Spin coating

Spin coating has been extensively explored in kesterite research, as it is well suited for processing of small substrates [2]. It typically involves the application of a liquid to a substrate, followed by the acceleration of the substrate up to a certain angular velocity rotational speed [120]. This method is typically combined with solutions of fairly low viscosity (< 0.01 Pa s) and it requires multiple depositions to build-up the necessary film thickness [117, 120]. The obtained film thickness depends on the angular velocity during deposition and the physical properties of the ink [120]. For obtaining a final film thickness on the order of 1–2 μm, a minimum of five successive layers are typically needed [12]. Despite the process simplicity, the low material utilization and the restriction to small substrates makes this method industrially less attractive [120]. Table 1 summarizes the record efficiencies obtained in CZTSSe to date with each coating method. Among the solution-based methods, the highest reposted efficiency of 12.6% was obtained using spin coating, and with hydrazine as the solvent [2] (see part (2.1) of the thin film synthesis section).

3.2. Spray coating

Spray coating is a method that is also compatible with low viscosity inks and it is suitable for large area deposition. This method involves forcing the ink through a nozzle to form a fine aerosol [120]. For the ink transport to the substrate, a carrier gas or electrostatic charging (electrostatic spraying) may be applied, and the spray jet is scanned continuously to cover the entire substrate area [81]. Although water would be the most benign and safest choice as the solvent, it may introduce substantial oxygen content in the final layer. Water also tends to be unsuitable for spray deposition due to its high surface tension, causing large droplet size and film disjoining upon drying. As a result, alcohol-based protic solvents have been the most commonly explored for spray coating, which allow for uniform films and fast solvent evaporation. However, the highest efficiency CZTSSe devices made by spray-coating employed either DMSO or DMF as a solvent, both of which have a surface tension substantially less than water, but higher than ethanol. The large number of drops in a spray deposition process, their varying velocity and droplet size with time due to evaporation and coalescence, and the temperature gradient between neighboring droplets, are typically so complex that computational resources fail to predict the dynamical and thermal interactions involved. Therefore, the optimum spray process parameters for obtaining device-grade kesterite films tend to be experimentally defined.

Spray coating can theoretically be used as a single coating method, as the solvent evaporates upon contact or in proximity to the substrate surface. In the CZTS system, however, it is only exploited as a two-step approach. The synthesis of kesterites-based absorber layers in an ambient environment using this technique was first reported by Nakayama in 1997 [121]. Following this work, different reports on the spray pyrolysis technique have been published, where the precursor type, substrate temperature, post thermal treatments and solution pH have been investigated [122–125]. The substrate temperature in particular, is a key process parameter, as it can influence both the morphology and the stoichiometry of the final film [126]. A drawback of this method is the relatively small grain size and high surface roughness, in comparison to other techniques [127]. The absorber roughness can directly influence the absorber/CdS interface, for solar cells prepared in the substrate configuration. This effect can be less detrimental for superstrate solar cells, where the kesterite is deposited on the CdS buffer layer. The relationship between secondary phase formation and chemical composition was also investigated [128]. It has been shown that non-optimum Cu/(Zn+Sn) and Zn/Sn compositional ratios can result in the formation of conductive secondary phases related to copper and sulfur compounds [128]. Spray processing generally leads to rougher films than other deposition methods, but offers several advantages over the

Table 1. A selected summary of the record power conversion efficiency values obtained from each deposition route, including the precursor type, any post-deposition treatments and self-reported efficiency limitations. PCE is total area, unless otherwise stated.

Solution/Nanoparticles	Coating	Precursor	Post-deposition step	Self-reported limitation	Efficiency
Solution (hydrazine)	Spin coating [2]	Zinc formate, Cu_2S/S, SnSe/Se, hydrazine	Annealing at $T > 500$ °C	Toxicity, Zn (S,Se) Secondary phases, Cu migration into $MoSe_2$	12.6%
Solution (aprotic)	Spin coating [49]	DMSO, thiourea, metal chlorides, metal acetates	Annealing in N_2, annealing in Se (graphite box)	None reported	11.5% 12.3% (active area)
Solution (aprotic)	Doctor blade [44]	DMSO, thiourea, metal chlorides, metal acetylacetonates	Annealing in Se	Fine-grained middle layer	10.3%
Solution (aprotic)	Spray [22]	DMF, thiourea, metal chlorides	Annealing in Se (graphite box)	Film roughness, plus inherent CZTSSe limitations.	11.0% (active area)
Suspension (protic)	Spray [60]	Cu–Zn–Sn sulfide colloid dispersed in water and ethanol	Annealing in N_2, annealing in Se	Porosity accelerating surface oxidation	10.8% (11.5%)[a] [119]
Suspension	Doctor blade [85]	CZTS NP dispersed in 1-hexanethiol	RTP in Se	Fine-grain layer after annealing	9.3%
Solution	Electro-deposition [115]	Metal sulfates in water	RTP in S	ZnS secondary phase, remaining fine-grain layer	8.7%

[a] IMRA Europe – publication in preparation.

more common spin- and dip-coating procedures, including reduced material loss during fabrication, higher sample throughput, and deposition over a larger area [81].

The highest efficiency CZTSSe PV device from a spray-coated molecular ink is 11.0% PCE and is based on DMF as a solvent [22]. Previous reports by the same group using DMSO achieved 9.5% PCE [129]. With regards to nanoparticle-based precursors, Larramona *et al* have reported an efficiency of 10.8% by (non-pyrolytic) spraying of a colloidal dispersion of CZTS nanoparticles in a solvent comprised of 90% water and 10% ethanol [60]. It is likely that these efficiencies (for both molecular inks and NP inks) will increase to similar levels as spin coated devices. As a case in point, a recent private communication reports that a 11.5% PCE device was achieved by the same team at IMRA for a 0.25 cm^2 total area small cell (so far unpublished data). This process was scaled to 1 cm^2 for a certified large area CZTSSe record of 9.8% PCE [84], and has now been pushed to 50 cm^2 [130]. The latter method has a high commercialization perspective due to the low toxicity of the precursors used.

3.3. Printing

Printing techniques, such as screen, pad and gravure printing describe a group of techniques where a layer of ink is transferred from a stamp to a substrate by a reversing action [120]. These techniques can have a very high throughput and offer the possibility of patterning. According to this definition, doctor blade and inkjet printing may rather be regarded as coating techniques, since they involve pouring or casting the ink, rather than stamping. However, they are included in this section as they share important features with more traditional printing methods; namely the compatibility with complex patterns, for the case of inkjet printing, and the necessity for high viscosity inks, for the case of doctor blading [131]. Inkjet printing is a highly versatile coating technique, as it allows deposition of both dissolved and dispersed inks, on any substrate. The working principle consists of the droplet formation and ejection, the spreading and coalescence of the droplets on a surface, and finally the solvent evaporation [131]. Inkjet printing offers the advantage of extremely high lateral resolution and roll-to-roll (R2R) compatibility. Its main disadvantages are its slow drying (compared to techniques like spin coating) and the requirement for very specific ink properties – namely viscosity and surface tension. Doctor blading involves a blade that moves over the substrate surface at a certain distance and at a constant velocity, spreading the ink. It offers high material utilization and it is easily transferrable to R2R, in the form of 'knife-over-edge' coating. Its main disadvantage is the necessity for high viscosity inks (> 100 mPa s), which generally requires additives [131].

Despite the versatility of these approaches, printing has not yet been substantially explored on the research scale for the CZTSSe system. In comparison to other coating methods, printing generally requires higher viscosity inks, in which case the viscosity adjustment is done using organic additives. The presence of the additives may leave carbon impurities in the film, thereby necessitating an additional high temperature annealing step for their removal. Especially when combined with the use of suspensions rather than solutions, long chain molecules are also used for the stabilization of the particles, which is an additional source of carbon in the film. This, together with the low yield for fabricating nanoparticles [132] can be regarded as the limitations for printing dispersed inks. The highest PCE achieved for CZTSSe films prepared using nanoparticle precursors is 9.3%, obtained using a doctor blading technique [85] (see the synthesis section nanoparticle part 2.4).

3.4. Electrodeposition (ED)

ED methods involve electron transfer reactions between electrodes and dissolved reactant ions, the latter usually being in an aqueous solution phase. To achieve uniform layers the reactant ions must arrive and reduce everywhere on the electrodes surface at the same rate, failure to do so leads to compositional and thickness non-uniformities likely resulting in secondary phase formation. The biggest advantage of these approaches is the low-cost, high uniformity and high material utilization efficiency exceeding 90% [133]. ED methods have already been successfully implemented in industry, which confirms their large area compatibility is possible [133]. In addition to the deposition of SELs, a 'one-pot' ED approach can be used, where all the elements (including S) are deposited in a single step. Still, a post-deposition annealing step must be performed to obtain highly crystalline and single phase material quality. The highest efficiency to date from ED was obtained using the co-electrodeposition approach, followed by RTP sulfurization [115]. This improved efficiency of 8.7% was achieved by increasing the background pressure during sulfurization. The increased partial pressure of sulfur during annealing has been shown to improve the crystallinity of the absorber and reduce the thickness of fine-grain layer [115].

4. SWOT analysis

Having reviewed the state-of-the-art solution-based strategies and the principal coating methods, it is worth comparing their relative strengths and weaknesses, as well as the possible opportunities and threats to future

Table 2. Comparison of the strengths, weaknesses, opportunities and threats for each of the different solution-based methods. It offers guidance for future research in that it highlights the relative promise and challenges that must be overcome for increased efficiency or for widespread implementation.

	Strength	Weakness	Opportunity	Threats
(1) Hydrazine-based suspensions and solutions	-Carbon-free solution leaves no residue -High efficiency 12.6% (IBM) -Continuously tunable composition -Does not require selenization (but does require high temperature anneal)	-Hydrazine is a dangerous and regulated solvent	-Enables synthesis of high quality absorber layers in order to carry out advanced characterization so that the material can be better understood	-Safety and environmental concerns with hydrazine if used for industrial purposes
(2) Aprotic molecular inks	-Simple ink preparation by dissolving salts -Continuously tunable composition -Relatively benign solvent (DMSO) used -High efficiency and reproducible across multiple labs, 11.8% (UW), 12.3% (Empa), 10.3% (ZSW)	-Highest efficiency preparations require 3 to 5 spin-coated layers plus annealing -Some (but not all) annealing profiles leave a carbon-rich layer or multilayer morphology -Requires selenization for high efficiency	-Ease of doping inks with other elements to passivate defects -Ease of scale-up by spray coating, blade-coating, or other deposition methods	-Controlling the thermal exposure during the annealing and selenization steps to remove C and N species and while forming dense grains.
(3) Protic solvents and the sol-gel method	-Simple ink preparation -Most environmentally friendly green solvents -Continuously tunable composition	-Metal oxide formation in the precursor requires reduction or aggressive selenization to remove oxide	-Ease of scale-up by spray coating, blade-coating, or other deposition methods	-Removal of O and C related impurities is challenging.
(4) Nanoparticle-Inks	-Tunable composition -Decouples primary kesterite formation from film deposition -Mild conditions for film deposition	>3 steps (Particle Synthesis, Ink Formulation, Film Deposition, Annealing) -Possible carbon residue from ligands on particles -Synthesis involves use of organic and inorganic compounds with foreign elements (Cl, O, C, N etc)	-Ease of scale-up by spray coating, blade-coating, or other deposition methods -Surface modification via ligand exchange to eliminate or reduce carbonaceous residue	-Presence of S due to incomplete conversion of CZTS nano-particles to CZTSe film -Maintaining uniformity of particles in scaled up synthesis
(5) Electrochemical coating	-Metal only deposition scalable to meter square areas -Low temperature operation -Stable benign precursor solutions which are recyclable	-Only applicable to conductive substrates -Some approaches yield extremely uneven coating even in small areas	-Roll-to-roll capabilities -For larger areas develop new (ED) cell geometry to improve current distribution and coating uniformity -Stacked elemental layer precursor can be used as a replacement to vacuum sputtered precursors	-Contaminants from bath or electrodes incorporated during the plating process -Uncontrollable precursor composition leading to detrimental secondary phase formation

research in these directions. A SWOT analysis is presented in table 2. The aim of this analysis is to highlight and offer guidance about the relative challenges faced by each route, rather than identifying a more suitable way over another. In general, except for perhaps the hydrazine-based approach, the detection/measurement and removal of impurities is still a topic which requires further research effort for all solution-based routes.

This analysis is explicitly based on solution methods, thus a direct comparison with vacuum or single crystal methods is avoided. However, even if not included in the table, an inherent strength of solution methods over vacuum methods is the high material utilization of Cu, Zn, and Sn. In comparison to vacuum-based methods, solution processes exhibit two main challenges. The first is to achieve reduced or impurity-free absorber layers, since impurities seem to be one of the factors which limit PCEs. The second relates to upscaling to industrially relevant sizes in an economically viable manner, which is proven for vacuum-based methods, but only somewhat for solution-based methods. Of course, the main challenge for all scientists working on the kesterite material is to further improve the PCE towards 20%.

5. Conclusion

For any photovoltaic absorber technology to succeed in the global marketplace, it must offer high performance, low-cost processing, and facile integration within existing manufacturing infrastructure. Kesterite-related technologies, most notably CZTSSe, have recently received a great deal of interest. The main reason for this is the performance increase achieved in laboratory-scale devices, as well as the high potential of this material system to serve as a 'drop-in' replacement for already commercialized CIGS absorbers. Key to this argument is the abundance/ low-cost of Zn, Sn raw materials (for substitution of rare and expensive In, Ga elements), and availability of cost-competitive approaches for fabricating the CZTSSe absorber layers. In this review, we have explored only an aspect of CZTSSe film processing that depends on liquid-based deposition. Such approaches not only provide a prospective pathway for low capital cost fabrication, but also the ability for depositing films of varying composition/morphology for defect and other chemical/physical studies, which are critical for overcoming current performance bottlenecks. While hydrazine-based approaches provided an early lead in terms of PV performance, at least in part because of the near-ideal solvent properties of hydrazine for chalcogenide-based materials, other less-toxic alternatives (based on protic, aprotic or nanoparticle-inks) have reached near parity. Overall, the leadership shown by liquid-based processing in terms of performance for the kesterite absorbers shows that such processing approaches provide a viable pathway for achieving state-of-the-art PCE values relative to vacuum-based approaches, which more typically are associated with high performance. However, in order for solution-based methods for CZTS to have further impact on the technology, an improvement in PCE towards >18% is required. Assuming this point is addressed, the combination of high performance and lower-cost liquid-based processing, coupled with readily-available metal component elements, should lead to a promising future for these technologies.

Acknowledgments

HWH acknowledges support from the US National Science Foundation (NSF) Sustainable Energy Pathway (SEP) award CHE-1230615 and NSF Division of Materials Research award DMR-1807541. SDD and RA acknowledge financial support from NSF under the Grant #1534691-DMR (DMREF) and #1735282-NRT (SUFEW). IMRA Europe acknowledge the European Commission for the funding on the kesterite research from 2017 by the H2020 programme under the project STARCELL (H2020-NMBP-03-2016-720907). MV acknowledges the financial support of Consejo Nacional de Investigaciones Científicas y Técnicas (CONICET, Argentina) and the Universidad Nacional de Mar del Plata (UNMdP, Argentina). DBM acknowledges financial support from the National Science Foundation under Grant No. 1511737. PA acknowledges financial support from the University of Luxembourg IRP LASER2. SA and ZS acknowledge H2020 EU Programme under the project INFINITE-CELL (H2020-MSCA-RISE-2017- 777968).

ORCID iDs

Z Sekkat https://orcid.org/0000-0002-2808-829X
S D Deshmukh https://orcid.org/0000-0001-7101-7393
R Agrawal https://orcid.org/0000-0002-6746-9829
P Arnou https://orcid.org/0000-0001-7992-0632
D B Mitzi https://orcid.org/0000-0001-5189-4612
P J Dale https://orcid.org/0000-0003-4821-8669

References

[1] Ito K and Nakazawa T 1988 Electrical and optical properties of stannite-type quaternary semiconductor thin films *Japan. J. Appl. Phys.* **27** 2094–7
[2] Wang W, Winkler M T, Gunawan O, Gokmen T, Todorov T K, Zhu Y and Mitzi D B 2014 Device characteristics of CZTSSe thin-film solar cells with 12.6% efficiency *Adv. Energy Mater.* **4** 1301465
[3] Ratz T *et al* 2019 Physical routes for the synthesis of kesterite *J. Phys. Energy* **4** 042003
[4] Friedlmeier T M, Wieser N, Walter T, Dittrich H and Schock H W 1997 Heterojunctions based on Cu_2ZnSnS_4 and $Cu_2ZnSnSe_4$ thin films *Proc. 14th European Conf. of Photovoltaic Science and Engineering and Exhibition* pp 1242–5
[5] Katagiri H, Jimbo K, Maw W S, Oishi K, Yamazaki M and Araki A T H 2009 Development of CZTS-based thin film solar cells *Thin Solid Films* **7** 2455–60
[6] Zoppi G, Forbes I, Miles R W, Dale P J, Scragg J J and Peter L M 2009 $Cu_2ZnSnSe_4$ thin film solar cells produced by selenisation of magnetron sputtered precursors *Prog. Photovolt. Res. Appl.* **17** 315–9
[7] Redinger A, Berg D M, Dale P J and Siebentritt S 2011 The consequences of kesterite equilibria for efficient solar cells *J. Am. Chem. Soc.* **133** 3320–3
[8] Mitzi D B, Kosbar L L, Murray C E, Copel M and Afzali A 2004 High-mobility ultrathin semiconducting films prepared by spin coating *Nature* **428** 299–303
[9] Mitzi D B, Yuan M, Liu W, Kellock A J, Jay Chey S, Deline V and Schrott A G 2008 A high-efficiency solution-deposited thin-film photovoltaic device *Adv. Mater.* **20** 3657–62
[10] Yuan M and Mitzi D B 2009 Solvent properties of hydrazine in the preparation of metal chalcogenide bulk materials and films *Dalton. Trans.* **31** 6078–88
[11] Todorov T K, Gunawan O, Gokmen T and Mitzi D B 2012 Solution-processed Cu(In, Ga)(S, Se)2 absorber yielding a 15.2% efficient solar cell *Prog. Photovolt. Res. Appl.* **21** 82–7
[12] Todorov T K, Reuter K B and Mitzi D B 2010 High-efficiency solar cell with earth-abundant liquid-processed absorber *Adv. Mater.* **22** E156–9
[13] Barkhouse D A R, Gunawan O, Gokmen T, Todorov T K and Mitzi D B 2012 Device characteristics of a 10.1% hydrazine-processed Cu 2ZnSn(Se, S) 4 solar cell *Prog. Photovoltaics. Res. Appl.* **20** 6–11
[14] Todorov T K, Tang J, Bag S, Gunawan O, Gokmen T, Zhu Y and Mitzi D B 2013 Beyond 11% efficiency: characteristics of state-of-the-art $Cu_2ZnSn(S, Se)4$ solar cells *Adv. Energy Mater.* **3** 34–8
[15] Todorov T, Sugimoto H, Gunawan O, Gokmen T and Mitzi D B 2014 High-Efficiency devices with pure solution-processed $Cu_2ZnSn(S, Se)4$ absorbers *IEEE J. Photovolt.* **4** 483–5
[16] Yang W, Duan H S, Bob B, Zhou H, Lei B, Chung C H, Li S H, Hou W W and Yang Y 2012 Novel solution processing of high-efficiency earth-abundant Cu 2ZnSn(S, Se)4 solar cells *Adv. Mater.* **24** 6323–9
[17] Winkler M T, Wang W, Gunawan O, Hovel H J, Todorov T K and Mitzi D B 2014 Optical designs that improve the efficiency of Cu2ZnSn(S,Se)4 solar cells *Energy Environ. Sci.* **7** 1029–36
[18] Ki W and Hillhouse W H 2011 Earth-abundant element photovoltaics directly from soluble precursors with high yield using a non-toxic solvent *Adv. Energy Mater.* **1** 732–5
[19] Xin H, Katahara K J, Braly L I and Hillhouse W H 2014 8% Efficient $Cu_2ZnSn(S, Se)4$ solar cells from redox equilibrated simple precursors in DMSO *Adv. Energy Mater.* **4** 1301823
[20] Xin H, Vorpahl S M, Collord A D, Braly I L, Uhl A R, Krueger B W, Ginger D S and Hillhouse H W 2015 Lithium-doping inverts the nanoscale electric field at the grain boundaries in Cu_2ZnSn (S, Se) 4 and increases photovoltaic efficiency *Phys. Chem. Chem. Phys.* **17** 23859–66
[21] Uhl A R, Katahara J K and Hillhouse H W 2016 Molecular-ink route to 13.0% efficient low-bandgap CuIn (S, Se)2 and 14.7% efficient Cu (In, Ga)(S, Se) 2 solar cells *Energy Environ. Sci.* **9** 130–4
[22] Collord A D and Hillhouse H W 2016 Germanium alloyed kesterite solar cells with low voltage deficits *Chem. Mater.* **28** 2067–73
[23] Tiwari D, Koehler T, Lin X, Sarua A, Harniman R, Wang L, Klenk R and Fermin D J 2017 Single molecular precursor solution for CuIn (S, Se) 2 thin films photovoltaic cells: structure AND device characteristics *ACS Appl. Mater. Interfaces* **9** 2301–8
[24] Uhl A R, Rajagopal A, Clark J A, Murray A, Feurer T, Buecheler S, Jen A K-Y and Hillhouse H W 2018 Solution-processed low-bandgap cuin (S, Se)2 absorbers for high-efficiency single-junction and monolithic chalcopyrite-perovskite tandem solar cells *Adv. Energy Mater.* **8** 1801254
[25] Liu F, Shen S, Zhou F, Song N, Wen X, Stride J A, Sun K, Yan C and Hao X 2015 Kesterite Cu_2ZnSnS_4 thin film solar cells by a facile DMF-based solution coating process *J. Mater. Chem.* C **3** 10783–92
[26] Su Z, Tan J M R, Li X, Zeng X, Batabyal S K and Wong L H 2015 Cation substitution of solution-processed Cu_2ZnSnS_4 thin film solar cell with over 9% efficiency *Adv. Energy Mater.* **5** 1500682
[27] Uhl A R, Fella C, Chiril/ua A, Kaelin M R, Karvonen L, Weidenkaff A, Borca C N, Grolimund D, Romanyuk Y E and Tiwari A N 2012 Non-vacuum deposition of Cu (In, Ga) Se2 absorber layers from binder free, alcohol solutions *Prog. Photovolt. Res. Appl.* **20** 526–33
[28] Zhao X, Lu M, Koeper M J and Agrawal R 2016 Solution-processed sulfur depleted Cu (In, Ga) Se2 solar cells synthesized from a monoamine—dithiol solvent mixture *J. Mater. Chem.* A **4** 7390–7
[29] Arnou P, Cooper C S, Uličná S, Abbas A, Eeles A, Wright L D, Malkov A V, Walls J M and Bowers J W 2017 Solution processing of CuIn (S, Se) 2 and Cu (In, Ga)(S, Se) 2 thin film solar cells using metal chalcogenide precursors *Thin Solid Films* **633** 76–80
[30] Fu J, Fu J, Tian Q, Wang H, Zhao F, Kong J, Zhao X and Wu S 2018 Tuning the Se content in Cu2ZnSn (S, Se) 4 absorber to achieve 9.7% solar cell efficiency from a thiol/amine-based solution process *ACS Appl. Energy Mater.* **1** 594–601
[31] Bordwell F G and Ji G Z 1991 Effects of structural changes on acidities and homolytic bond dissociation energies of the H–N bonds in amidines, carboxamides, and thiocarboxamides *J. Am. Chem. Soc.* **113** 8398–401
[32] Bowmaker G A, Hanna J V, Pakawatchai C, Skelton B W, Thanyasirikul Y and White A H 2008 Crystal structures and vibrational spectroscopy of copper (I) thiourea complexes *Inorg. Chem.* **48** 350–68
[33] Spofford W A and Amma E L 1970 The crystal structure of bis (thiourea) copper (I) chloride *Acta Crystallogr.* B **26** 1474–83
[34] Vizzini E A, Taylor I F and Amma E L 1968 Electron-deficient bonding with sulfur atoms: III. Crystal and molecular structure of bis (thiourea) silver (I) chloride *Inorg. Chem.* **7** 1351–7
[35] Madarász J, Bombicz P, Okuya M and Kaneko S 2001 Thermal decomposition of thiourea complexes of Cu (I), Zn (II), and Sn (II) chlorides as precursors for the spray pyrolysis deposition of sulfide thin films *Solid State Ionics* **141** 439–46
[36] Olmstead W N, Margolin Z and Bordwell F G 1980 Acidities of water and simple alcohols in dimethyl sulfoxide solution *J. Org. Chem.* **45** 3295–9

[37] Clark J A, Murray A, Lee J M, Autrey T S, Collord A D and Hillhouse H W 2019 Complexation chemistry in n, n-dimethylformamide-based molecular inks for chalcogenide semiconductors and photovoltaic devices *J. Am. Chem. Soc.* **141** 298–308

[38] Kim S, Kim K M, Tampo H, Shibata H and Niki S 2016 Improvement of voltage deficit of Ge-incorporated kesterite solar cell with 12.3% conversion efficiency *Appl. Phys. Express* **9** 102301

[39] Giraldo S *et al* 2015 Large efficiency improvement in $Cu_2ZnSnSe_4$ solar cells by introducing a superficial Ge nanolayer *Adv. Energy Mater.* **5** 1501070

[40] Ford G M, Guo Q, Agrawal R and Hillhouse H W 2011 Earth abundant element Cu_2 $Zn(Sn_{1-x}Ge_x)S_4$ nanocrystals for tunable band gap solar cells: 6.8% efficient device fabrication *Chem. Mater.* **23** 2626–9

[41] Qi Y, Tian Q, Meng Y, Kou D, Zhou Z, Zhou W and Wu S 2017 Elemental precursor solution processed $(Cu_{1-x}Ag_x)$ 2ZnSn (S, Se) 4 photovoltaic devices with over 10% efficiency *ACS Appl. Mater. Interfaces* **9** 21243–50

[42] Gershon T, Lee Y S, Antunez P, Mankad R, Singh S, Bishop D, Gunawan O, Hopstaken M and Haight R 2016 Photovoltaic materials and devices based on the alloyed kesterite absorber (Ag_xCu_{1-x}) $2ZnSnSe_4$ *Adv. Energy Mater.* **6** 1502468

[43] Qi Y-F, Kou D-X, Zhou W-H, Zhou Z-J, Tian Q-W, Meng Y-N, Liu X-S, Du Z-L and Wu S-X 2017 Engineering of interface band bending and defects elimination via a Ag-graded active layer for efficient (Cu, Ag) 2 ZnSn (S, Se) 4 solar cells *Energy Environ. Sci.* **10** 2401–10

[44] Schnabel T, Abzieher T, Friedlmeier T M and Ahlswede E 2015 Solution-based preparation of Cu2ZnSn(S,Se)4 for solar cells—comparison of SnSe2 and elemental Se as chalcogen source *IEEE J. Photovolt.* **5** 670–5

[45] Werner M, Keller D, Haass S G, Gretener C, Bissig B, Fuchs P, La Mattina F, Erni R, Romanyuk Y E and Tiwari A N 2015 Enhanced carrier collection from CdS passivated grains in solution-processed Cu 2 ZnSn(S,Se) 4 solar cells *ACS Appl. Mater. Interfaces* **7** 12141–6

[46] Abzieher T, Schnabel T, Hetterich M, Powalla M and Ahlswede E 2016 Source and effects of sodium in solution-processed kesterite solar cells *Phys. Status Solidi Appl. Mater. Sci.* **213** 1039–49

[47] Clark J A, Uhl A R, Martin T R and Hillhouse H W 2017 Evolution of morphology and composition during annealing and selenization in solution-processed $Cu_2ZnSn(S, Se)_4$ *Chem. Mater.* **29** 9328–39

[48] Haass S G, Diethelm M, Werner M, Bissig B, Romanyuk Y E and Tiwari A N 2015 11.2% efficient solution processed kesterite solar cell with a low voltage deficit *Adv. Energy Mater.* **5** 1500712

[49] Haass S G, Andres C, Figi R, Schreiner C, Bürki M, Romanyuk Y E and Tiwari A N 2018 Complex interplay between absorber composition and alkali doping in high-efficiency kesterite solar cells *Adv. Energy Mater.* **8** 1701760

[50] Tanaka K, Moritake N and Uchiki H 2007 Preparation of Cu2 ZnSnS4 thin films by sulfurizing sol-gel deposited precursors *Sol. Energy Mater. Sol. Cells* **91** 199–201

[51] Sakka S 1985 Sol-gel synthesis of glasses: present and future *Am. Ceram. Soc. Bull.* **64** 1463–6

[52] Su Z, Sun K, Han Z, Cui H, Liu F, Lai Y, Li J, Hao X, Liu Y and Green M A 2014 Fabrication of Cu_2ZnSnS_4 solar cells with 5.1% efficiency via thermal decomposition and reaction using a non-toxic sol-gel route *J. Mater. Chem.* A **2** 500–9

[53] Sun K, Yan C, Liu F and Hao X 2018 Towards 9% sulfide CZTS solar cells fabricated by a sol-gel process *2018 IEEE 7th World Conf. on Photovoltaic Energy Conversion, WCPEC 2018—A Joint Conf. of 45th IEEE PVSC, 28th PVSEC and 34th EU PVSEC* pp 0856–8

[54] Laghfour Z *et al* 2016 Thickness effect on Cu_2ZnSnS_4 properties using non-toxic and low-cost process *2016 Int. Renewable and Sustainable Energy Conf. (IRSEC)* pp 792–4

[55] Habas S E, Platt H A S, van Hest M F A M and Ginley D S 2010 Low-cost inorganic solar cells: from ink to printed device *Chem. Rev.* **110** 6571–94

[56] Bucherl C N, Oleson K R and Hillhouse H W 2013 Thin film solar cells from sintered nanocrystals *Curr. Opin. Chem. Eng.* **2** 168–77

[57] Wang D, Zhao W, Zhang Y and Liu S 2018 (Frank) Path towards high-efficient kesterite solar cells *J. Energy Chem.* **27** 1040–53

[58] Wu W, Tassi N G, Cao Y, Caspar J V, Roy-Choudhury K and Zhang L 2015 Optoelectronic characteristics of >9% efficient bilayered CuZnSn(S,Se)4 photovoltaic device *Phys. Status Solidi—Rapid Res. Lett.* **9** 236–40

[59] Hages C J, Levcenco S, Miskin C K, Alsmeier J H, Abou-Ras D, Wilks R G, Bär M, Unold T and Agrawal R 2015 Improved performance of Ge-alloyed CZTGeSSe thin-film solar cells through control of elemental losses *Prog. Photovolt. Res. Appl.* **23** 376–84

[60] Larramona G, Levcenko S, Bourdais S, Jacob A, Choné C, Delatouche B, Moisan C, Just J, Unold T and Dennler G 2015 Fine-tuning the Sn content in CZTSSe thin films to achieve 10.8% solar cell efficiency from spray-deposited water-ethanol-based colloidal inks *Adv. Energy Mater.* **5** 1501404

[61] Hages C J and Agrawal R 2015 Synthesis of CZISSe thin films from nanocrystal inks *Copper Zinc Tin Sulfide-based Thin Film Solar Cells* ed K Ito (New York: Wiley) pp 239–70

[62] Bourdais S, Chone C and Cuccaro Y 2017 Large-grain crystallized metal chalcogenide film, colloidal solution of amorphous particles, and preparation methods *US Patent Specification* 9,731,262 B2

[63] Larramona G, Bourdais S, Jacob A, Choné C, Muto T, Cuccaro Y, Delatouche B, Moisan C, Péré D and Dennler G 2014 Efficient Cu_2ZnSnS_4 solar cells spray coated from a hydro-alcoholic colloid synthesized by instantaneous reaction *RSC Adv.* **4** 14655–62

[64] Guo Q, Hillhouse H W and Agrawal R 2009 Synthesis of Cu_2ZnSnS_4 nanocrystal ink and its use for solar cells *J. Am. Chem. Soc.* **131** 11672–3

[65] Riha S C, Parkinson B A and Prieto A L 2009 Solution-based synthesis and characterization of Cu_2ZnSnS_4 nanocrystals *J. Am. Chem. Soc.* **131** 12054–5

[66] Steinhagen C, Panthani M G, Akhavan V, Goodfellow B, Koo B and Korgel B A 2009 Synthesis of Cu_2ZnSnS_4 nanocrystals for use in low-cost photovoltaics *J. Am. Chem. Soc.* **131** 12554–5

[67] Guo Q, Kim S J, Kar M, Shafarman W N, Birkmire R W, Stach E A, Agrawal R and Hillhouse H W 2008 Development of $CuInSe_2$ nanocrystal and nanoring inks for low-cost solar cells *Nano Lett.* **8** 2982–7

[68] Ghorpade U, Suryawanshi M, Shin S W, Gurav K, Patil P, Pawar S, Hong C W, Kim J H and Kolekar S 2014 Towards environmentally benign approaches for the synthesis of CZTSSe nanocrystals by a hot injection method: a status review *Chem. Commun.* **50** 11258–73

[69] Guo Q, Ford G M, Yang W C, Hages C J, Hillhouse H W and Agrawal R 2012 Enhancing the performance of CZTSSe solar cells with Ge alloying *Sol. Energy Mater. Sol. Cells* **105** 132–6

[70] Collord A D and Hillhouse H W 2015 Composition control and formation pathway of CZTS and CZTGS nanocrystal inks for kesterite solar cells *Chem. Mater.* **27** 1855–62

[71] Hages C J, Koeper M J and Agrawal R 2016 Optoelectronic and material properties of nanocrystal-based CZTSe absorbers with Ag-alloying *Sol. Energy Mater. Sol. Cells* **145** 342–8

[72] Lu X, Zhuang Z, Peng Q and Li Y 2011 Wurtzite Cu_2ZnSnS_4 nanocrystals: a novel quaternary semiconductor *Chem. Commun.* **47** 3141–3

[73] Regulacio M D, Ye C, Lim S H, Bosman M, Ye E, Chen S, Xu Q H and Han M Y 2012 Colloidal nanocrystals of wurtzite-type Cu_2ZnSnS_4: facile noninjection synthesis and formation mechanism *Chem.—Eur. J.* **18** 3127–31

[74] Yang W C, Miskin C K, Hages C J, Hanley E C, Handwerker C, Stach E A and Agrawal R 2014 Kesterite $Cu_2ZnSn(S, Se)4$ absorbers converted from metastable, wurtzite-derived Cu_2ZnSnS_4 nanoparticles *Chem. Mater.* **26** 3530–4

[75] Chianelli R R and Dines M B 1978 Low-Temperature solution preparation of group 4B, 5B and 6B transition-metal dichalcogenides *Inorg. Chem.* **17** 2758–62

[76] Schulz D L, Curtis C J, Flitton R A, Wiesner H, Keane J, Matson R J, Jones K M, Parilla P A, Noufi R and Ginley D S 1998 Cu-In-Ga-Se nanoparticle colloids as spray deposition precursors for Cu(In, Ga)Se2 solar cell materials *J. Electron. Mater.* **27** 433–7

[77] Yang W C, Miskin C K, Carter N J, Agrawal R and Stach E A 2014 Compositional inhomogeneity of multinary semiconductor nanoparticles: a case study of Cu_2ZnSnS_4 *Chem. Mater.* **26** 6955–62

[78] Miskin C K, Yang W, Hages C J, Carter N J, Joglekar C S, Stach E A and Agrawal R 2015 9.0% efficient $Cu_2ZnSn(S, Se)$ 4 solar cells from selenized nanoparticle inks *Prog. Photovolt. Res. Appl.* **23** 654–9

[79] Guo Q *et al* 2012 A simple solution-based route to high-efficiency CZTSSe thin-film solar cells *Conf. Record of the IEEE Photovoltaic Specialists Conf.* (Piscataway, NJ: IEEE) pp 2993–6

[80] Shinde N M, Dubal D P, Dhawale D S, Lokhande C D, Kim J H and Moon J H 2012 Room temperature novel chemical synthesis of Cu_2ZnSnS_4 (CZTS) absorbing layer for photovoltaic application *Mater. Res. Bull.* **47** 302–7

[81] Patil P S 1999 Versatility of chemical spray pyrolysis technique *Mater. Chem. Phys.* **59** 185–98

[82] Foos E E, Yoon W, Lumb M P, Tischler J G and Townsend T K 2013 Inorganic photovoltaic devices fabricated using nanocrystal spray deposition *ACS Appl. Mater. Interfaces* **5** 8828–32

[83] Schulz D L, Curtis C J, Cram A, Alleman J L, Mason A, Matson R J, Perkins J D and Ginley D S 1997 ClGS Films via nanoparticle spray deposition: attempts at densifying a porous precursor *1997 26th IEEE Photovoltaic Specialists Conf.* pp 483–6

[84] Green M A, Emery K, Hishikawa Y, Warta W and Dunlop E D 2016 Solar cell efficiency tables (version 48) *Prog. Photovolt. Res. Appl.* **24** 905–13

[85] Hages C J, Koeper M J, Miskin C K, Brew K W and Agrawal R 2016 Controlled grain growth for high performance nanoparticle-based kesterite solar cells *Chem. Mater.* **28** 7703–14

[86] Deligianni H, Romankiw L T, Lincot D and Grand P-P 2018 From the lab to scaling-up thin film solar absorbers *Electrochemical Engineering: From Discovery to Product* (*Advances in Electrochemical Sciences and Engineering*) (New York: Wiley-VCH Verlag GmbH & Co. KGaA) pp 75–128

[87] Scragg J J, Dale P J and Peter L M 2008 Towards sustainable materials for solar energy conversion: preparation and photoelectrochemical characterization of Cu_2ZnSnS_4 *Electrochem. Commun.* **10** 639–42

[88] Peter L M 2015 Electrochemical routes to earth-abundant photovoltaics: a minireview *Electrochem. Commun.* **50** 88–92

[89] Colombara D, Crossay A, Vauche L, Jaime S, Arasimowicz M, Grand P P and Dale P J 2015 Electrodeposition of kesterite thin films for photovoltaic applications: Quo vadis? *Phys. Status Solidi Appl. Mater. Sci.* **212** 88–102

[90] Araki H, Kubo Y, Jimbo K, Maw W S, Katagiri H, Yamazaki M, Oishi K and Takeuchi A 2009 Preparation of Cu_2ZnSnS_4 thin films by sulfurization of co-electroplated Cu–Zn–Sn precursors *Phys. Status Solidi Curr. Top. Solid State Phys.* **6** 1266–8

[91] Ahmed S, Reuter K B, Gunawan O, Guo L, Romankiw L T and Deligianni H 2012 A high efficiency electrodeposited Cu_2ZnSnS_4 solar cell *Adv. Energy Mater.* **2** 253–9

[92] Yuan T, Li Y, Jia M, Lai Y, Li J, Liu F and Liu Y 2015 Fabrication of Cu_2ZnSnS_4 thin film solar cells by sulfurization of electrodeposited stacked binary Cu–Zn and Cu–Sn alloy layers *Mater. Lett.* **155** 44–7

[93] Lehner J, Ganchev M, Loorits M, Revathi N, Raadik T, Raudoja J, Grossberg M, Mellikov E and Volobujeva O 2013 Structural and compositional properties of CZTS thin films formed by rapid thermal annealing of electrodeposited layers *J. Cryst. Growth* **380** 236–40

[94] Khalil M I, Atici O, Lucotti A, Binetti S, Le Donne A and Magagnin L 2016 CZTS absorber layer for thin film solar cells from electrodeposited metallic stacked precursors (Zn/Cu-Sn) *Appl. Surf. Sci.* **379** 91–7

[95] Guo L, Zhu Y, Gunawan O, Gokmen T, Deline V R, Ahmed S, Romankiw L T and Deligianni H 2014 Electrodeposited $Cu_2ZnSnSe_4$ thin film solar cell with 7% power conversion efficiency *Prog. Photovolt. Res. Appl.* **22** 58–68

[96] Vauche L, Risch L, Sánchez Y, Dimitrievska M, Pasquinelli M, Goislard De Monsabert T, Grand P P, Jaime-Ferrer S and Saucedo E 2016 8.2% pure selenide kesterite thin-film solar cells from large-area electrodeposited precursors *Prog. Photovolt. Res. Appl.* **24** 38–51

[97] Yao L, Ao J, Jeng M J, Bi J, Gao S, Sun G, He Q, Zhou Z, Sun Y and Chang L B 2017 A CZTSe solar cell with 8.2% power conversion efficiency fabricated using electrodeposited Cu/Sn/Zn precursor and a three-step selenization process at low Se pressure *Sol. Energy Mater. Sol. Cells* **159** 318–24

[98] Jiang F, Ikeda S, Harada T and Matsumura M 2014 Pure sulfide Cu_2ZnSnS_4 thin film solar cells fabricated by preheating an electrodeposited metallic stack *Adv. Energy Mater.* **4** 1301381

[99] Jiang F, Ikeda S, Tang Z, Minemoto T, Septina W, Harada T and Matsumura M 2015 Impact of alloying duration of an electrodeposited Cu/Sn/Zn metallic stack on properties of Cu_2ZnSnS_4 absorbers for thin-film solar cells *Prog. Photovolt. Res. Appl.* **23** 1884–95

[100] Dale P J, Malaquias J C and Steichen M 2014 Semiconductors for photovoltaic devices: electrochemical approaches using ionic liquids *ECS Trans.* **58** 1–12

[101] Steichen M, Malaquias J C, Arasimowicz M, Djemour R, Brooks N R, Van Meervelt L, Fransaer J, Binnemans K and Dale P J 2017 High-speed electrodeposition of copper-tin-zinc stacks from liquid metal salts for $Cu_2ZnSnSe_4$ solar cells *Chem. Commun.* **53** 913–6

[102] Clauwaert K, Goossens M, De Wild J, Colombara D, Dale P J, Binnemans K, Matthijs E and Fransaer J 2016 Electrodeposition and selenization of brass/tin/germanium multilayers for Cu 2 $Zn(Sn_{1-x}Ge_x)Se_4$ thin film photovoltaic devices *Electrochim. Acta* **198** 104–14

[103] Pawar B S, Pawar S M, Shin S W, Choi D S, Park C J, Kolekar S S and Kim J H 2010 Effect of complexing agent on the properties of electrochemically deposited Cu_2ZnSnS_4 (CZTS) thin films *Appl. Surf. Sci.* **257** 1786–91

[104] Gougaud C, Rai D, Delbos S, Chassaing E and Lincot D 2013 Electrochemical studies of one-step electrodeposition of Cu–Sn–Zn layers from aqueous electrolytes for photovoltaic applications *J. Electrochem. Soc.* **160** D485–94

[105] Perelstein G, Valdes M and Vazquez M 2019 Different routes of fixed pH to electrodeposit Cu_2ZnSnS_4 for photovoltaic devices *Materialia* **5** 100187

[106] Khalil M I, Bernasconi R and Magagnin L 2014 CZTS layers for solar cells by an electrodeposition-annealing route *Electrochim. Acta* **145** 154–8

[107] Chaudhari S, Palli S, Kannan P K and Dey S R 2016 Pulsed electrodeposition of Cu_2ZnSnS_4 absorber layer precursor for photovoltaic application *Thin Solid Films* **600** 169–74

[108] Clauwaert K, Binnemans K, Matthijs E and Fransaer J 2016 Electrochemical studies of the electrodeposition of copper-zinc-tin alloys from pyrophosphate electrolytes followed by selenization for CZTSe photovoltaic cells *Electrochim. Acta* **188** 344–55
[109] Unveroglu B and Zangari G 2017 Effect of cell configuration on the compositional homogeneity of electrodeposited Cu–Zn–Sn alloys and phase purity of the resulting Cu_2ZnSnS_4 absorber layers *Electrochim. Acta* **255** 347–57
[110] Rovelli L, Tilley S D and Sivula K 2013 Optimization and stabilization of electrodeposited Cu_2ZnSnS_4 photocathodes for solar water reduction *ACS Appl. Mater. Interfaces* **5** 8018–24
[111] Shao P W, Li C T, Ho K C and Cheng K W 2015 Catalytic and photoelectrochemical performances of Cu–Zn–Sn–Se thin films prepared using selenization of electrodeposited Cu–Zn–Sn metal precursors *J. Power Sources* **286** 47–57
[112] Jeon J O *et al* 2014 Highly efficient copper-zinc-tin-selenide (CZTSe) solar cells by electrodeposition *ChemSusChem.* **7** 1073–7
[113] Valdés M, Hernández-Martinez A, Sánchez Y, Oliva F, Izquierdo-Roca V, Perez Rodriguez A and Saucedo E 2018 $Cu_2ZnSnSe_4$ based solar cells combining co-electrodeposition and rapid thermal processing *Sol. Energy* **173** 955–63
[114] Ge J, Jiang J, Yang P, Peng C, Huang Z, Zuo S, Yang L and Chu J 2014 A 5.5% efficient co-electrodeposited ZnO/CdS/Cu_2ZnSnS_4/Mo thin film solar cell *Sol. Energy Mater. Sol. Cells* **125** 20–6
[115] Zhang C, Tao J and Chu J 2018 An 8.7% efficiency co-electrodeposited Cu_2ZnSnS_4 photovoltaic device fabricated via a pressurized post-sulfurization process *J. Mater. Chem.* C **6** 13275–82
[116] Ge J and Yan Y 2018 Controllable multinary alloy electrodeposition for thin-film solar cell fabrication: a case study of kesterite Cu_2ZnSnS_4 *iScience* **1** 55–71
[117] Romanyuk Y E, Fella C M, Uhl A R, Werner M, Tiwari A N, Schnabel T and Ahlswede E 2013 Recent trends in direct solution coating of kesterite absorber layers in solar cells *Sol. Energy Mater. Sol. Cells* **119** 181–9
[118] Todorov T K and Mitzi D B 2010 Direct liquid coating of chalcopyrite light-absorbing layers for photovoltaic devices *Eur. J. Inorg. Chem.* **2010** 17–28
[119] Larramona G, Bourdais S, Jacob A, Choné C, Moisan C, Delatouche and Péré D 2019 Development of CZTS thin film solar cell made with aqueous colloidal ink spray: from cells to record mini-modules (in preparation)
[120] Krebs F C 2009 Fabrication and processing of polymer solar cells: a review of printing and coating techniques *Sol. Energy Mater. Sol. Cells* **93** 394–412
[121] Nakayama N and Ito K 1996 Sprayed films of stannite Cu_2ZnSnS_4 *Appl. Surf. Sci.* **92** 171–5
[122] Seboui Z, Cuminal Y and Kamoun-Turki N 2013 Physical properties of Cu_2ZnSnS_4 thin films deposited by spray pyrolysis technique *J. Renew. Sustain. Energy* **5** 023113
[123] Dermenji L *et al* 2017 Effects of annealing on elemental composition and quality of CZTSSe thin films obtained by spray pyrolysis *Surf. Eng. Appl. Electrochem.* **52** 509–14
[124] Courel M, Picquart M, Arce-Plaza A, Pulgarin-Agudelo F A, González-Castillo J R, Montoya De Los Santos I and Vigil-Galán O 2018 Study on the impact of stoichiometric and optimal compositional ratios on physical properties of Cu_2ZnSnS_4 thin films deposited by spray pyrolysis *Mater. Res. Express* **5** 015513
[125] Kim S and Kim J 2013 Effect of selenization on sprayed $Cu_2ZnSnSe_4$ thin film solar cell *Thin Solid Films* **547** 178–80
[126] Perednis D and Gauckler L J 2005 Thin film deposition using spray pyrolysis *J. Electroceram.* **14** 103–11
[127] Serin T, Serin N, Karadeniz S, Sari H, Tuğluoğlu N and Pakma O 2006 Electrical, structural and optical properties of SnO_2 thin films prepared by spray pyrolysis *J. Non. Cryst. Solids* **352** 209–15
[128] Vigil-Galán O, Espíndola-Rodríguez M, Courel M, Fontané X, Sylla D, Izquierdo-Roca V, Fairbrother A, Saucedo E and Pérez-Rodríguez A 2013 Secondary phases dependence on composition ratio in sprayed Cu_2ZnSnS_4 thin films and its impact on the high power conversion efficiency *Sol. Energy Mater. Sol. Cells* **117** 246–50
[129] Collord A D, Xin H and Hillhouse H W 2015 Combinatorial exploration of the effects of intrinsic and extrinsic defects in $Cu_2ZnSn(S, Se)4$ *IEEE J. Photovolt.* **5** 288–98
[130] Brammertz G, Meissner D, Larramona G, Bras P and Ren Y 2019 Reliability and possible technological applications of Kesterite solar cells *J. Phys. Energy*
[131] Burgués-Ceballos I, Stella M, Lacharmoise P and Martínez-Ferrero E 2014 Towards industrialization of polymer solar cells: material processing for upscaling *J. Mater. Chem.* A **2** 17711–22
[132] Panthani M G, Akhavan V, Goodfellow B, Schmidtke J P, Dunn L, Dodabalapur A, Barbara P F and Korgel B A 2008 Synthesis of $CuInS_2$, $CuInSe_2$, and $Cu(In_xGa_{1-x})Se_2$ (CIGS) nanocrystal 'inks' for printable photovoltaics *J. Am. Chem. Soc.* **130** 16770–7
[133] Deligianni H, Ahmed S and Romankiw L T 2016 The next frontier: electrodeposition for solar cell fabrication *Interface Mag.* **20** 47–53